





Supramolecular spheres assembled from covalent and supramolecular dendritic crowns dictate the supramolecular orientational memory effect mediated by Frank-Kasper phases

Ning Huang^a, Mohammad R. Imam^{a,b}, Monika J. Sienkowska^a, Mihai Peterca^a, Marian N. Holerca^a, Daniela A. Wilson^{a,c}, Brad M. Rosen^a, Benjamin E. Partridge^{a,d}, Qi Xiao^a, Virgil Percec^{a,*}

Keywords: Frank–Kasper phases, Supramolecular orientational memory, Conical and crown dendrons and dendrimers, Distorted dodecahedral architecture, Discriminating mechanisms

A supramolecular orientational memory (SOM) effect that provides access to complex columnar hexagonal architectures that cannot be designed by any other methodology was recently reported by our laboratory. This SOM concept is encountered upon heating and cooling a hexagonal columnar periodic array via a Frank–Kasper phase that is generated from supramolecular spheres. Here, a library of twenty-four supramolecular spheres self-organizing into Frank–Kasper phases and columnar hexagonal arrays was investigated for SOM. Twenty of these supramolecular spheres, that were self-assembled from conical shaped dendrons, did not exhibit SOM. The four supramolecular spheres assembled from covalent and supramolecular dynamic crowns displayed SOM. The supramolecular dynamic crowns forming spheres by a strong and directional H-bonding process, generated *via* SOM, a previously unencountered distorted dodecahedral architecture constructed from hexagonally ordered supramolecular columns. Therefore, SOM can discriminate between mechanisms of self-assembly of supramolecular spheres, a process that cannot be accomplished by analysis with X-ray diffraction methods alone. These results will facilitate access to the design of new complex columnar hexagonal and other periodic columnar array architectures *via* SOM.

Introduction

The elucidation of the hierarchical mechanisms of emergence, corruption and loss of memory, and the discovery of new memory effects represent some of the greatest challenges of natural

E-mail address: percec@sas.upenn.edu (V. Percec).

Received 12 March 2020; Received in revised form 18 March 2020; Accepted 20 March 2020

^a Roy and Diana Vagelos Laboratories, Department of Chemistry, University of Pennsylvania, Philadelphia, Pennsylvania 19104-6323, United States

^b Department of Mathematics and Natural Sciences American University of Iraq, Sulaimani (AUIS) Sulaimania, Kurdistan Region 46001, Iraq

^c Institute for Molecules and Materials, Radboud University, Heyendaalseweg 135, 6525 AJ Nijmegen, The Netherlands

^d Department of Chemistry and International Institute for Nanotechnology, Northwestern University, Evanston, Illinois 60208, United States

 $^{^{\}ast}\,$ Corresponding author.

sciences. Memory is one of the most fundamental and complex functions of biological, synthetic and societal complex systems that involves the process by which information is encoded, stored and retrieved when needed. In the medical field some of the most challenging problems to be solved are the Alzheimer's and Prion diseases that are considered to be associated with the erroneous folding of β -sheets and their aggregation into toxic fibrils and prions [1–6]. In synthetic systems memory effects were observed in the early days of the previous century. Shape memory of AuCd alloys was discovered in 1932 [7] and since then has been observed in other alloys, ceramics and metals [8–11]. Memory in soft condensed matter provided shape memory polymers [12–14] with biomedical applications [15]. Orientational memory provided the widely used technology of liquid crystal displays [16–18]. Chiral memory is a more recent event discovered [19–22].

The most recently discovered memory effect is the supramolecular orientational memory (SOM) effect [23-25]. A detailed description of this memory concept will be presented in a different part of the manuscript. The first SOM effect was discovered upon heating at the transition from the columnar hexagonal array of supramolecular dendrimers to their $Pm\bar{3}n$ cubic or A15 Frank-Kasper phase and cooling back to their columnar hexagonal phase [23]. A second example of SOM was observed at the transition from the columnar hexagonal phase of supramolecular dendrimers to their $Im\bar{3}n$ body centered cubic (BCC) phase and back to their columnar hexagonal array [24]. In both cases a covalent crown-conformation of a selfassembling dendrimer was found to be responsible for the SOM effect. These two examples of SOM provided access, for the first time, to complex orthogonal and tetrahedral arrangements of columnar hexagonal periodic arrays. It is expected that the elucidation of the hierarchical mechanism of emergence of SOM from supramolecular columnar hexagonal and other

columnar assemblies to all cubic, quasicrystal and Frank-Kasper phases of supramolecular dendrimers [23-28] will generate a new synthetic methodology to self-organize unprecedentedly complex arrangements of supramolecular assemblies in soft condensed matter. Novel functions are expected to derive from them. Since Frank-Kasper phases were also discovered in block copolymers, giant molecules and surfactants, it is expected that SOM may be a general concept that could facilitate access to new morphologies and functions. Cubic A15 and BCC phases, quasicrystals and Frank-Kasper phases are generated from spherical supramolecular dendrimers. Two mechanisms of self-assembly of spherical supramolecular dendrimers are currently available: from a fragment of a sphere the smallest one being a conical-shape and from a covalent crown-shape. This manuscript will first search through libraries of conical and crown self-assembling dendrimers to elucidate if both of these two conformers form spheres that facilitate the SOM effect. Since the SOM experiments reported so far were performed with covalent crown-conformers generated spheres, the second experiment will address the supramolecular spheres generated from supramolecular dynamic crown-conformers. The results of these experiments will facilitate access to the design of the SOM effect both in supramolecular dendrimers as well as in other supramolecular systems forming Frank-Kasper phases.

Methods

Differential scanning calorimetry (DSC)

Thermal transitions were measured on TA instrument 2920 modulated, and Q 100 DSC integrated with a refrigerated cooling system (RCS). The heating, and cooling rates were $10\,^{\circ}$ C/min. The transition temperatures were measured as the maxima, and minima of their endothermic, and exothermic peaks. Indium was used as calibration standard.

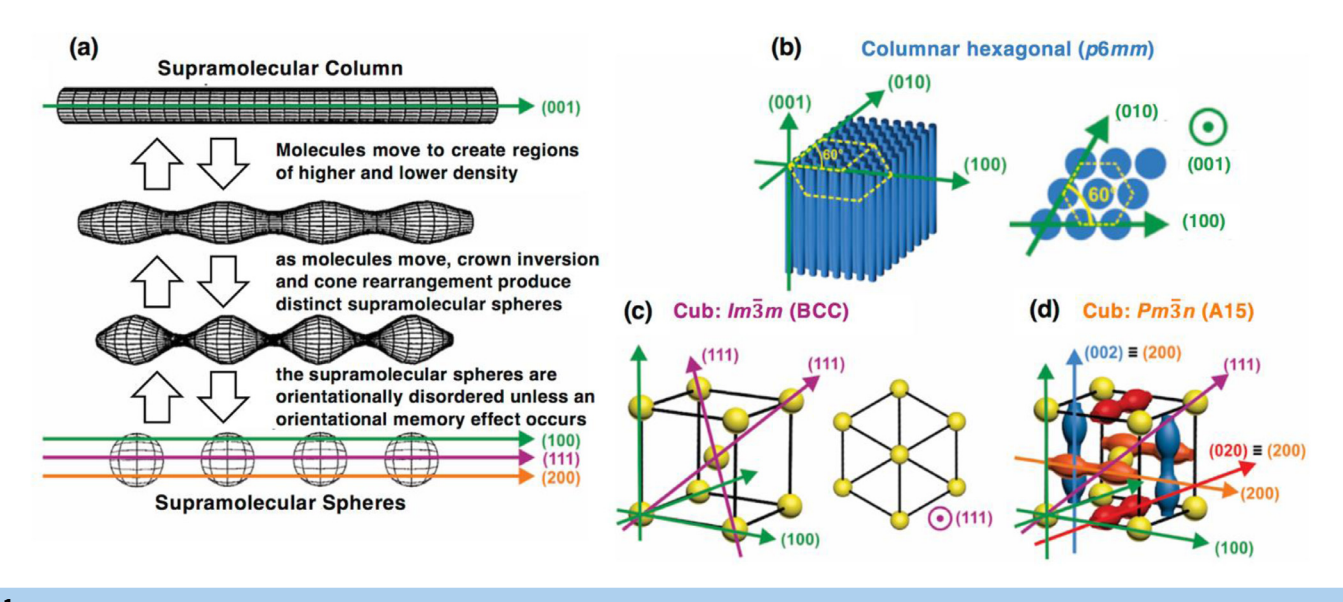


Fig.

The mechanism (a) of reversible transformation of supramolecular columns from a columnar hexagonal assembly (b) into supramolecular spheres (a) present in BCC (c) and $Pm\bar{3}n$ or A15 Frank–Kasper (d) periodic arrays. The close contact spheres in the BCC (c) and A15 (d) are indicated with colored arrows together with their (100), (111), or (200) directions indicated at the end of the arrow. These are the close contact sphere directions or continuous supramolecular spheres in cubic lattices that were demonstrated by electron density maps [44,45,50] shown with the colored arrows in the bottom part of panel (a).

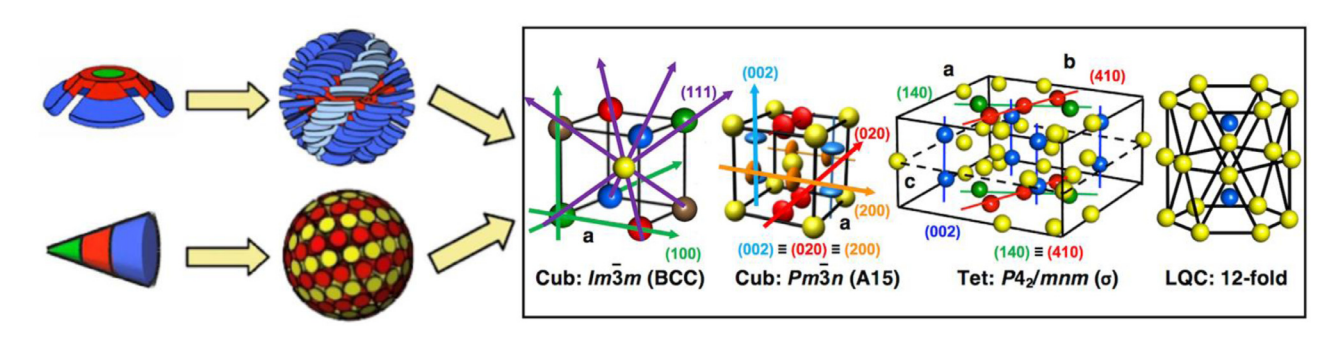


Fig. 2

Self-organization of conical and crown-like conformations of dendrons and dendrimers into chiral spheres and their BCC, A15, σ and liquid quasicrystal (LQC) assemblies. The closed contact spheres are colored, and their direction is shown by an arrow.

Fiber preparation

Well-aligned fiber was made by using a custom extrusion device. About 10 mg of samples were aligned in solid state with force subjected during extrusion at 25 °C for fiber preparation (Figure S1). Heat may be needed to make well-aligned fibers from time to time. A heater was used for 3–5 s to heat up the sample powder before extrusion. Fibers were loaded in a capillary to carry out XRD experiments. In general, the thickness of the extruded fiber is around 0.5 mm and the length is around 5 mm. All XRD experiments were carried out with fiber axis perpendicular to the beam direction.

X-ray diffraction (XRD)

XRD measurements were performed in the two following X-ray scarttering facilities.

Multi-angle X-ray scattering facility (MAXS)

XRD experiments were conducted by using Cu-K\$\alpha\$ radiation (\$\lambda\$ =1.54178 Å) from a Bruker-Nonius FR-591 rotating anode X-ray source equipped with a 0.2 × 0.2 mm² filament operated at 3.4 kW. The radiation from Cu target was collimated and focused with Osmic\$^{TM}\$ confocal optics followed by circular pinholes, and a Bruker Hi-Star\$^{TM}\$ multiwire (area) detector was used to detect the scattered radiation. An integral vacuum was maintained along the length of the flight tube and within the sample chamber view the view to minimizing attenuation and background scattering. Samples were held in thin glass capillaries (1.0 mm in diameter), mounted in a temperature-controlled oven (temperature precision: $\pm 0.1\,^{\circ}\text{C}$, temperature range from $-120\,^{\circ}\text{C}$ to $270\,^{\circ}\text{C}$). The sample-to-detector distance was kept at 54.0 cm with a \$q\$-range of 0.02–0.38 Å\$^{-1}\$.

Dual-source and environmental X-ray scattering facility (DEXS)

XRD experiments were conducted by using Cu-K $_{\alpha 1}$ radiation ($\lambda = 1.54178\,\text{Å}$) from Xeuss 2.0 with the slits of $1.2 \times 1.2\,\text{mm}$ for high flux and $0.7 \times 0.7\,\text{mm}$ for high resolution. To minimize attenuation, and background scattering, an integral vacuum was maintained along the length of the flight tube, and within the sample chamber. Samples were held in glass

capillaries (1.0 mm in diameter), mounted in a temperature controlled oven (temperature precision: \pm 0.1 °C, temperature range: from –10 to 210 °C). Aligned samples for fiber XRD experiments were prepared using a custom-made extrusion device. Powdered sample (~10 mg) was heated inside the extrusion device. Sample-to-detector distance was 550 mm. Additional measurements to verify indexed parameters were performed with a sample-to-detector distance of 160 mm. Primary XRD analysis was performed using Datasqueeze (version 3.0.5).

Results and discussion

A brief discussion to the Frank–Kasper phases and quasicrystals in soft condensed matter

Frank-Kasper phases were discovered in metal alloys containing d-orbitals and reported in 1958 [29] and 1959 [30] by Sir Charles Frank and Kasper. Subsequently they were discovered in the condensed phases of small molecules such as N_2 [31–36], CO [37] and O_2 [38-41], in lipids [42,43], in supramolecular dendrimers [44,45] and in self-organizable dendronized polymers [46]. Soon after these discoveries the $Pm\bar{3}n$ periodic array known also as the Frank-Kasper A15 phase was discovered in numerous libraries of quasiequivalent constitutional isomeric supramolecular dendrimers [47-71] and the prediction of the primary structure of self-assembling dendron and dendrimer forming this phase was immediately elucidated via quasiequivalent constitutional isomeric building blocks. Spherical supramolecular dendrimers are the first examples of monodisperse supramolecular polymers. The discovery of spherical supramolecular dendrimers forming the A15 Frank-Kasper phase was inspired by the structure and the elucidation of the mechanism of self-assembly of icosahedral and rod-like viruses by Aaron Klug [72]. A brief history of this discovery was written by invitation [73]. The discovery of the Frank-Kasper A15 phase in supramolecular dendrimers instigated theoretical and molecular dynamic simulation experiments [74–76]. The discovery of supramolecular spherical dendrimers that self-organize in tetragonal lattice symmetry P42/mnm or σ Frank-Kasper phase [77] and quasicrystals [78] followed. All these phases were also discovered in self-organizable dendronized polymers [70]. In 2010 Bates laboratory reported the discovery of the σ Frank–Kasper phase in block copolymers [79,80]. This was

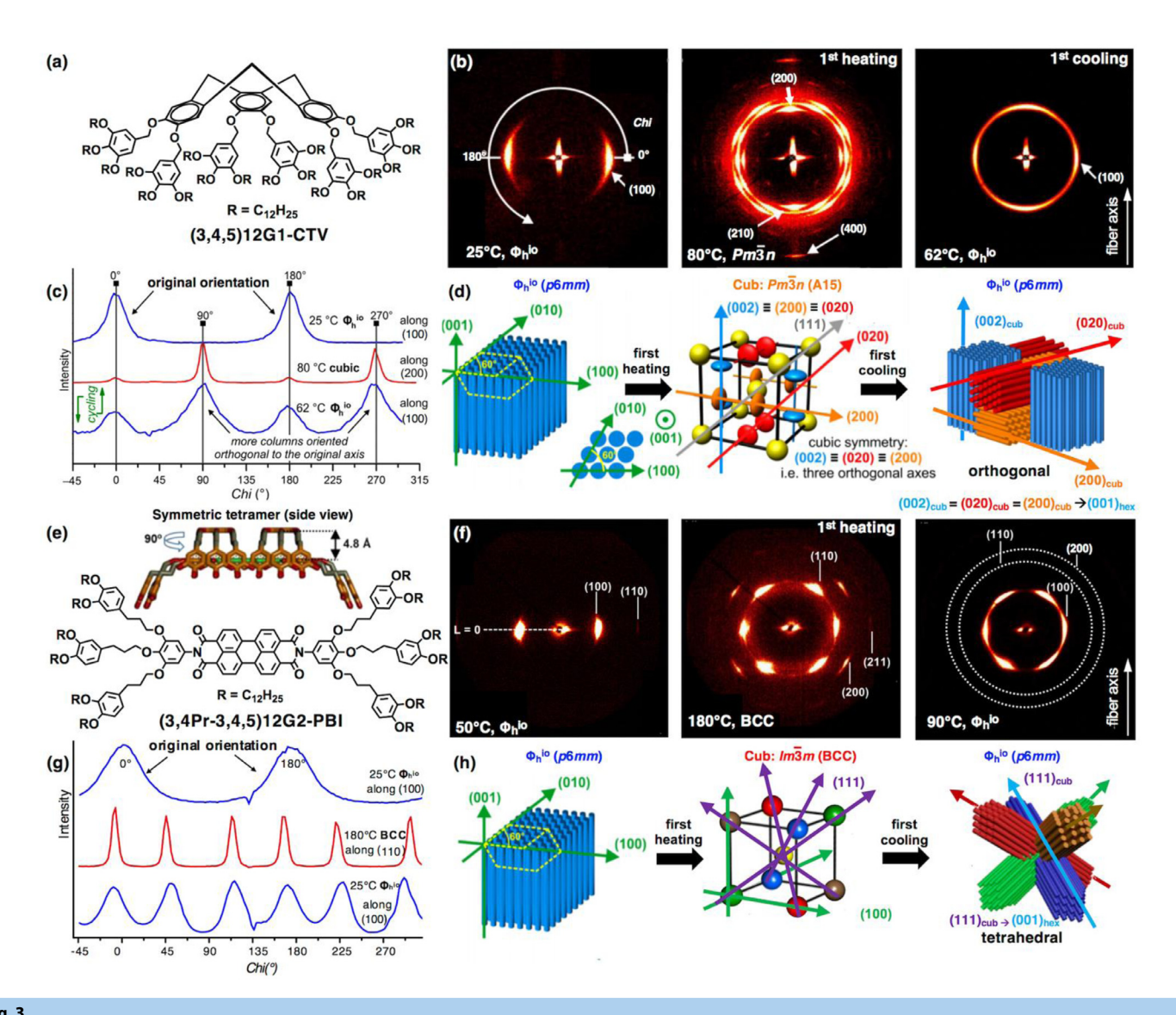


Fig. 3

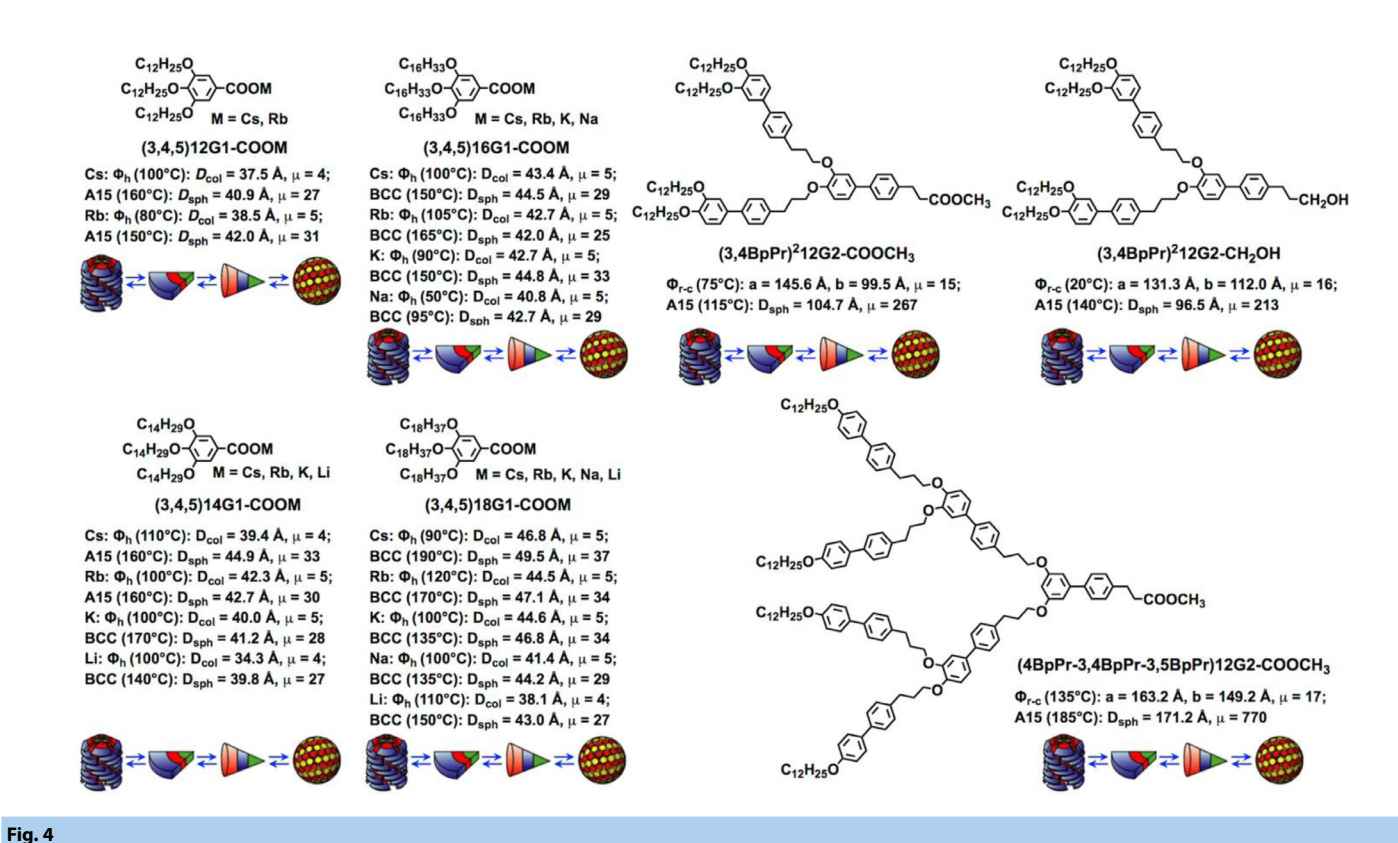
Structural and retrostructural analysis of supramolecular assemblies generated from the self-assembling (3,4,5)12G1-CTV (a) and (3,4Pr-3,4,5)12G2-PBI (e) crowns by small-angle x-ray diffraction (XRD) experiments (b, f) performed on oriented fibers obtained by extrusion at 25 °C along the (001)_{hex} direction. Azimuthal plot of the XRD patterns in (b) along (100)_{hex} and (200)_{cub} (c). Schematic representation of the transition from columnar hexagonal with intracolumnar order Φ_h^{io} (p6mm) to cubic ($Pm\bar{3}n$, A15) lattice on first heating and cooling to generate the supramolecular orientational memory effect that results in an orthogonal architecture of columns arranged in a Φ_h^{io} array (d). Close-contact spheres are colored in blue, red and orange in the cubic unit cell and are responsible for the formation of the orthogonal architecture of columns. XRD of the assemblies of (3,4Pr-3,4,5)12G2-PBI (e) are shown in (f). Azimuthal plot of the patterns from (f) are in (g) along (100) and (110) directions. Schematic representation of the lattice transition between columnar hexagonal with intracolumnar order Φ_h^{io} (p6mm) and cubic (BCC) lattice on first heating and cooling (g). The transition from Φ_h^{io} to the BCC array with its close-contact spheres colored in blue, red, green and brown are responsible for the formation of tetrahedral arrangement of columns upon cooling (h). (For interpretation of the references to color in this figure legend, the reader is referred to the web version of this article.)

soon followed by the discovery of the quasi-crystal phase in block copolymers [81] and the C14, C15 Frank–Kasper phases also in block copolymers [82]. In 2013 the Frank–Kasper A15 phase was discovered also in surfactants by the Mahanthappa laboratory [83]. In subsequent years the same laboratory discovered the σ [84], C14 and C15 [85] phases in surfactants. In 2015 Cheng laboratory discovered the Frank–Kasper A15 phase in giant surfactants [86]. The similar giant molecules provided the σ [87], quasicrystal [88] phases, and the Z phase [89]. Recently, DNA complexes [90] and sugar-polyolefin block copolymers [91,92] with Frank–Kasper phases were reported. The advantage

of working with self-assembling dendrons and dendrimers is their monodisperse structure that provides access to first order phase transitions in both differential scanning calorimetry (DSC) and X-ray diffraction experiments [26].

Hierarchical mechanism of reversible transformation of columnar to spherical supramolecular dendrimers

Fig. 1 outlines this mechanism of reversible transformation of columnar to spherical supramolecular dendrimers. The molecules in the supramolecular columns move to create regions of higher and lower electron density and ultimately produce orientationally



Structural and retrostructural analysis of supramolecular dendrimers self-assembled from conical carboxylate salts conformers and conical biphenylpropyl ether conformers. Short notations and summary of these results are explained in Table 1 and part of Table 2.

disordered spheres. This process is reversible and corresponds to a first order phase transition (Fig. 1a).

If the columns are self-organized in a columnar hexagonal periodic array (Fig. 1b) and the transition transforms the supramolecular columns into supramolecular spheres self-organized in BCC (Fig. 1c) or A15 (Fig. 1d) phases a SOM process may occur. This is mediated by the fact that the supramolecular spheres are not only arranged in the BCC lattice symmetry but because the spheres on the four (111) directions of the BCC lattice are in closer contact than the corner centered spheres in between themselves (Fig. 1c) [53]. In the A15 phase the pairs of spheres from the (200), (020) and (002) [44] are also in closer contact than all other spheres of the A15 unit cell (Fig. 1d). The close contact spheres from BCC and A15 can mediate a preferential orientation of the columns from the columnar hexagonal (*p*6mn) phase that are generated at the first order phase transitions from the BCC and A15 phases.

Fig. 2 shows the two mechanisms via which supramolecular spheres forming the BCC, A15, σ , and quasicrystal (LQC) are formed. Both mechanisms of self-assembly from crown- and conical-shaped dendrons and dendrimers self-organize chiral spheres that can be racemic or homochiral [62–64,71] and the directions of the close contact spheres on all these lattices are indicated in Fig. 2. The role and the mechanism of the transfer of chirality from column to sphere during SOM is not yet known and therefore, it will not be discussed here.

The currently known mechanisms of SOM mediated by covalent crowns

The two currently elucidated mechanisms of SOM mediated with covalent dendrimers, dendronized cyclotriveratrylene (CTV), (3,4,5)12G1-CTV (Fig. 3a), from columnar hexagonal (*p6mn*) to A15 (Fig. 3a to d) [23] and dendronized perylene bisimide (PBI) (3,4Pr-3,4,5)12G2-PBI (Fig. 3e) from p6mn to BCC (Fig. 3e-h) [24,25] are summarized in Fig. 3.

These experiments were performed with fibers of supramolecular columnar hexagonal assemblies oriented by extrusion at 25 °C in the p6mm phase. The oriented fiber pattern of the small angle X-rays (XRD) are shown in the left XRD panels from Fig. 3b and f. The orientation of the columns along the (001) direction of the columnar hexagonal phase is observed. Upon heating to the A15 and BCC phases we can see oriented spheres diffraction on the (200), (020), and (002) directions that corresponds to the close-contact spheres in A15 and the closecontact (111) direction in the BCC phases. Upon cooling from the A15 and BCC phases back to the columnar hexagonal phase we see a 4-fold symmetry for the (100)_{hex} diffraction in the case of the A15-mediated SOM and a 6-fold symmetry of the (100)_{hex} for the case of the BCC-mediated SOM. These diffractions are explained by the orthogonal arrangement of hexagonal columns generated by the A15 SOM (Fig. 3d) and tetrahedral arrangement of hexagonally oriented columns in the case of the BCC-mediated SOM (Fig. 3h). A more detailed description of this orientation process is illustrated in Fig. 3c and g.

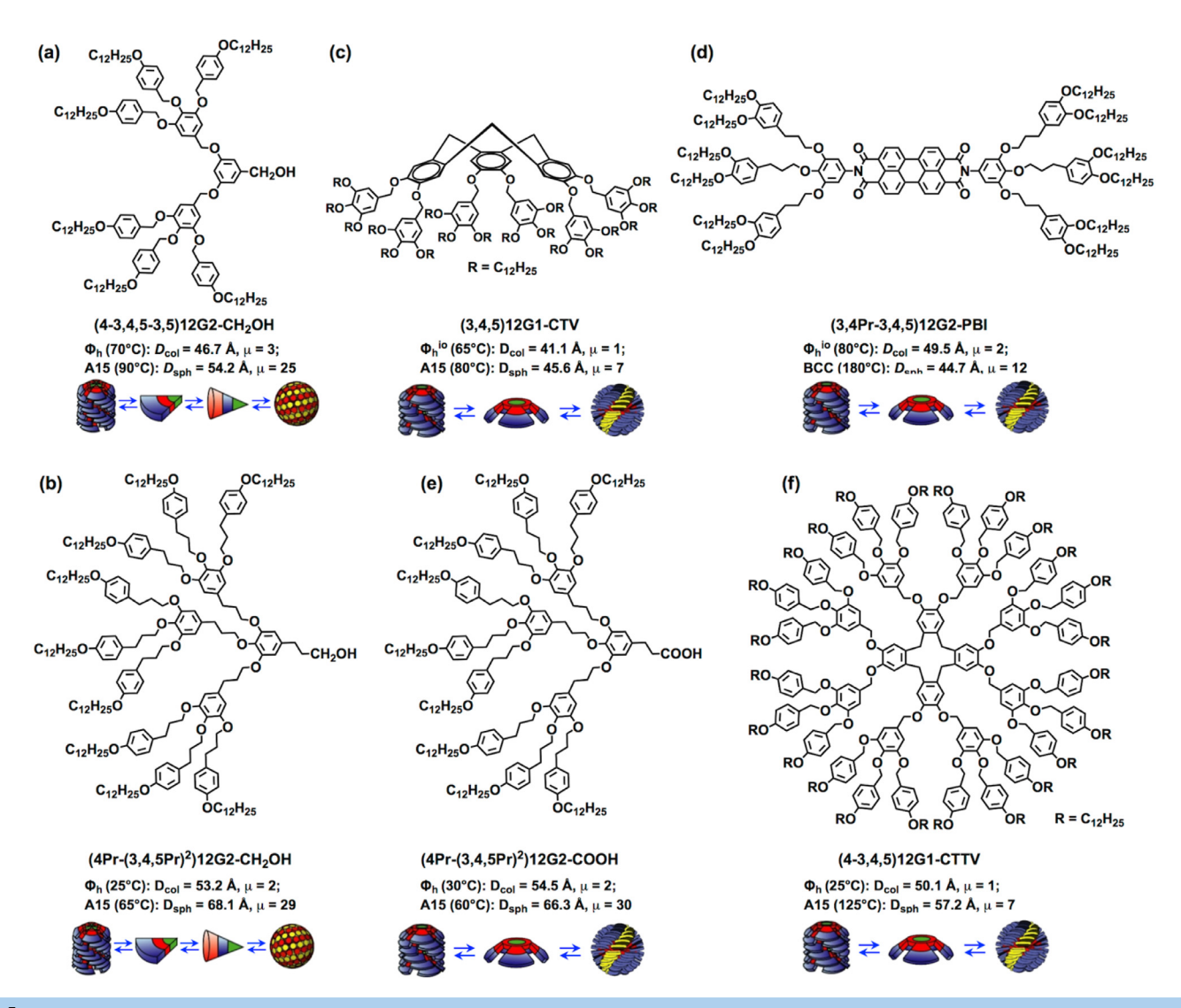


Fig. 5

The results of the structural and retrostructural analysis of supramolecular dendrimers self-assembled from conical conformers of benzyl ether (a) and phenylpropyl ether (b) both containing $-CH_2OH$ at the apex, self-assembling covalent crown dendrimer conformers of dendronized cyclotriveratrylene (c), dendronized perylene bisimide (d), supramolecular crown of phenylpropyl ether containing -COOH at the apex (e), and covalent crown of dendronized cyclotetraveratrylene (f). Short notations and summary of these results are explained in Table 2.

For A15 SOM from (3,4,5)12G1-CTV, the orientations of $(200)_{cub}$, $(020)_{cub}$, and $(002)_{cub}$ axes of the close-contact supramolecular spheres in the A15 phase are preserved in the columnar hexagonal array, becoming (100)hex directions for orthogonally-oriented columnar domains (Fig. 3d). The 4-fold symmetry patterns located at 0°, 90°, 180°, and 270° in the azimuthal plot of the (100) reflection after cooling (Fig. 3c, lower blue line) indicate alignment of supramolecular columns along the (200)_{cub}, (020)_{cub}, and (002)_{cub} axes of the preceding A15 unit cell. Different from cubic powder XRD, the formation of the cubic phase originates from a well-aligned fiber along the (001) direction of the Φ_h^{io} that excludes the reflections from random orientation distributions and, therefore, the correlations of the equivalent axes can be reflected in the azimuthal plot in contrast to a uniform ring obtained from the powder XRD. In other words, the XRD pattern is similar to the single domain cubic lattice. The reason for the four-fold symmetry pattern is attributed to the fact that (200)_{cub}, (020)_{cub}, and (002)_{cub} are perpendicular to each other in the unit cell and the azimuthal plot reflects the correlation between each axis. Close-contact spheres, colored in blue, red, and orange, are aligned along the (200)_{cub}, (020)_{cub}, and (002)_{cub} axes and will dominate the orientation of column formation upon cooling. The distance between two close-contact spheres is $0.5 \times a$ along the $(200)_{cub}$ axis. Azimuthal plots of the XRD patterns (Fig. 3c) indicate that (200)_{cub} and its equivalent axes dictate the directions of the column formation. Hence, upon heating, the (001)_{hex} orientation of the aligned fiber becomes the (002)_{cub} axis of the cubic unit cell, as shown by four peaks in the azimuthal plot along the (200) direction at 80 °C. Upon subsequent cooling, the newly formed columnar hexagonal lattice preserves the orientation of the (200)_{cub} with four distinctive peaks in the azimuthal plot along the (100)_{hex} corresponding to the $(200)_{\text{cub}}$ and its equivalent axes in the previous $Pm\bar{3}n$ lattice. A four-fold pattern was observed in the XRD scattering at 62 °C (Fig. 2b), which further confirms the preservation of the orientation from cubic lattice to columnar hexagonal array.

For BCC SOM from (3,4Pr-3,4,5)12G2-PBI, the close-contact spheres in the BCC lattice are instead aligned along the (111)_{cub} axis [24], which is the body diagonal of the unit cell (Fig. 3h). Upon cooling from the BCC lattice at 180 °C, the (111)_{cub} axis and its equivalent axes dictate the orientation of the (001)_{hex} direction of the supramolecular columns, giving a six-fold symmetry in the XRD pattern (Fig. 3f). Azimuthal plots of the XRD patterns along (110)_{cub} and (100)_{hex} also provide strong evidence for the preservation of the orientations in the columnar hexagonal array from the previous BCC lattice (Fig. 3g). Distinct from the orthogonal architecture generated by cooling an A15 Frank–Kasper cubic lattice, in which orientation is preserved from (200)_{cub} to (001)_{hex}, the orientational memory effect from the BCC cubic lattice preserves

the (111)_{cub} direction to give a complex tetrahedral nanoscale architecture.

Searching for SOM from conical vs covalent crown derived supramolecular spheres

In order to address the role of the conformation of the secondary structure of the dendron or dendrimer in the generation of the SOM effect a library of 15 conical carboxylate salts conformers (3,4,5)nG1-COOM with n=12, and M=Cs, Rb; n=14, M=Cs, Rb, K, Li; n=16, M=Cs, Rb, K, Na; and n=18, M=Cs, Rb, K, Na, Li that all display a transition from supramolecular A15 to BCC were investigated (first two columns from the left side of Fig. 4) [55].

Fig. 4 contains a total of 18 molecules displaying conical conformations in their spherical supramolecular dendrimers. The details of the structural and retrostructural analysis of the first 15 supramolecular assemblies are summarized in Table 1. Three additional conical dendrons $(3,4BpPr)^212G2\text{-}COOCH_3$, $(3,4BpPr)^212G2\text{-}CH_2OH$ and $(4BpPr-3,4BpPr-3,5\text{-}BpPr)12G2\text{-}COOCH_3$ that self-organize in columnar hexagonal and A15

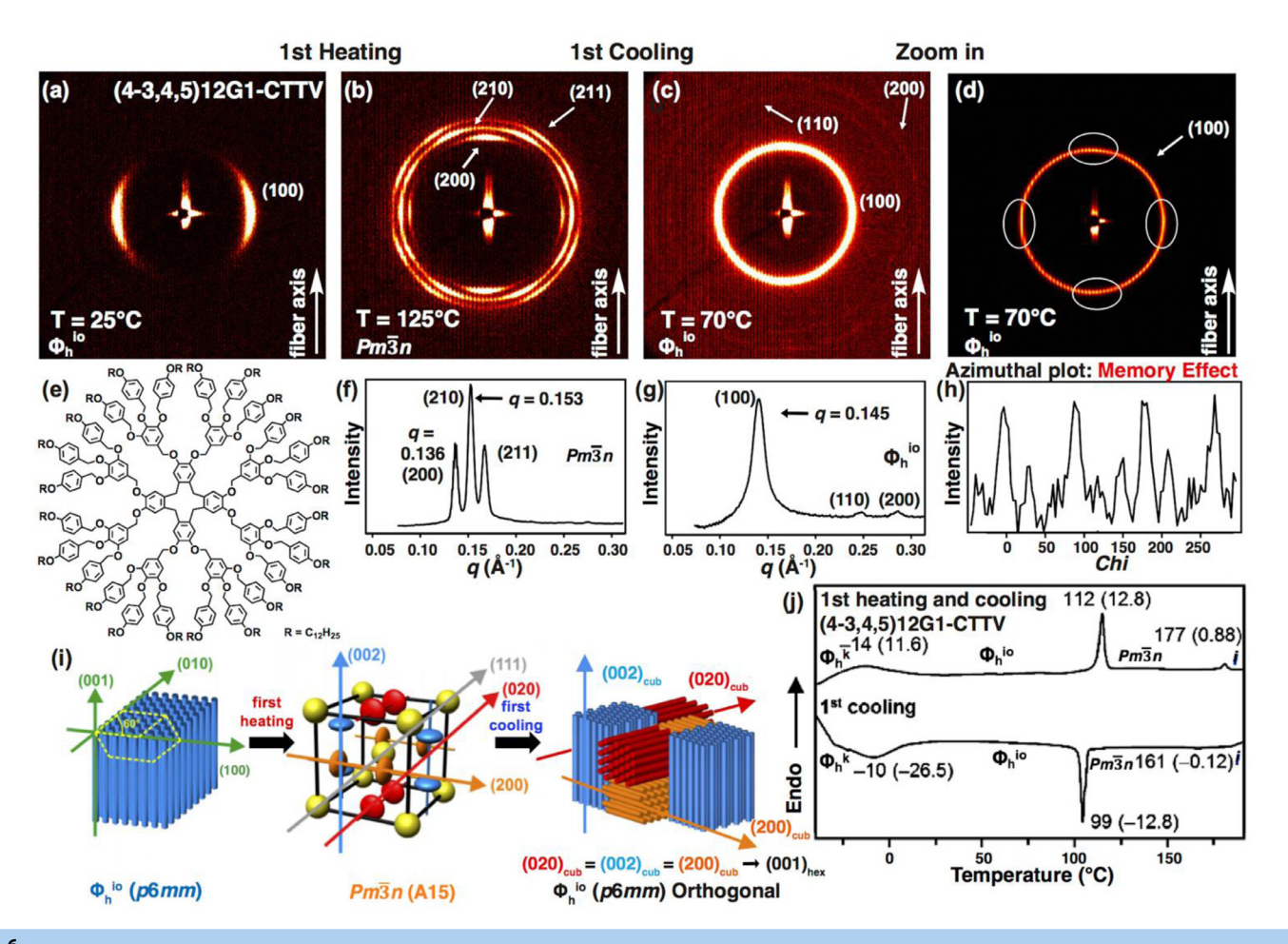


Fig. 6

Structural and retrostructural analysis by small-angle XRD on first heating and cooling scans of fiber aligned by extrusion at 25 °C (a,b,c,d) of the supramolecular assemblies of the crown conformer of (4-3,4,5)12G1-CTTV (e); XRD plots of $Pm\bar{3}n$ (A15) and Φ_h (p6mm) periodic arrays (f, g). Azimuthal plot of the patterns in (d) along $(100)_{hex}$ (h). Schematic representation of the transition between columnar hexagonal Φ_h (p6mm) and cubic ($Pm\bar{3}n$, A15) lattices on first heating and cooling showing the orthogonal arrangements of hexagonal columns generated by the supramolecular orientational memory effect (i). Close-contact spheres are colored in blue, red and orange in the cubic unit cell and are providing the driving force for the formation of complex arrangements of orthogonal columns upon cooling. DSC traces of first heating and cooling at 10 °C/min (j). Phases indexed by XRD, transition temperatures (in °C), and associated enthalpy changes (in parentheses in kcal/mol) are shown on the DSC traces. (For interpretation of the references to color in this figure legend, the reader is referred to the web version of this article.)

Table 1

Structural Analysis of Conical Carboxylate Salts Conformers of Self-Assembling Dendrons by Small-Angle XRD to Search for the Orientational Memory Effect.

No	Molecule	T (°C)	Phase ^a	d_{100} , d_{110} , d_{200} $(\mathring{A})^b$ d_{110} , d_{200} , d_{211} $(\mathring{A})^c$ d_{200} , d_{210} , d_{211} $(\mathring{A})^d$	a, b, c (Å) ^e	D _{col} ^f / D _{sph} ^g (Å)	μ	Memory Effect
1								
		100	Φ_{h}	32.6, 18.7, 16.2 ^b	37.5, 37.5, –	37.5 f	4 ^h	
2	(3,4,5)12G1-COORb	150	Pm3n	34.1, 29.7, 28.0 ^d	67.7, 67.7, 67.7	42.0 9	31 ⁱ	No
		80	Φ_{h}	33.2, 19.2, 16.6 ^b	38.5, 38.5, –	38.5 f	5 h	
3	(3,4,5)14G1-COOCs	160	Pm3n	36.2, 32.3, 29.5 ^d	72.3, 72.3, 72.3	44.9 9	33 ⁱ	No
		110	Φ_{h}	34.3, 19.6, 17.0 ^b	39.4, 39.4, –	39.4 f	4 ^h	
4	(3,4,5)14G1-COORb	160	Pm3n	34.3, 30.7, 28.0 ^d	68.8, 68.8, 68.8	42.7 9	30 ⁱ	No
		100	Φ_{h}	36.7, 21.2, 18.2 ^b	42.3, 42.3, -	42.3 f	5 h	
5	(3,4,5)14G1-COOK	170	BCC	29.6, 20.9, 17.0 ^c	41.8, 41.8, 41.8	41.2 9	28 ⁱ	No
		100	Φ_{h}	34.7, 19.9, 17.3 ^b	40.0, 40.0, -	40.0 f	5 h	
6	(3,4,5)14G1-COOLi	140	BCC	28.4, 20.3, 16.5 ^c	40.4, 40.4, 40.4	39.8 9	27 ⁱ	No
		100	Φ_{h}	29.6, 17.3, 14.8 ^b	34.3, 34.3, -	34.3 ^f	4 ^h	
7	(3,4,5)16G1-COOCs	150	BCC	31.9, 22.7, 18.4 ^c	45.2, 45.2, 45.2	44.5 9	29 ⁱ	No
		100	Φ_{h}	37.3, 21.7, 19.0 ^b	43.4, 43.4, -	43.4 f	5 h	
8	(3,4,5)16G1-COORb	165	BCC	31.8, 22.7, 18.4 ^c	42.6, 42.6, 42.6	42.0 9	25 i	No
		105	Φ_{h}	36.9, 21.4, 18.5 ^b	42.7, 42.7, –	42.7 f	5 h	
9	(3,4,5)16G1-COOK	150	BCC	32.1, 22.7, 18.6 ^c	45.5, 45.5, 45.5	44.8 9	33 ⁱ	No
		90	Φ_{h}	37.0, 21.5, 18.6 ^b	42.7, 42.7, –	42.7 f	5 h	
10	(3,4,5)16G1-COONa	95	BCC	30.8, 21.7, 17.7 ^c	43.4, 43.4, 43.4	42.7 9	29 ⁱ	No
		50	Φ_{h}	35.6, 20.7, 17.8 ^b	40.8, 40.8, -	40.8 ^f	5 h	
11	(3,4,5)18G1-COOCs	190	BCC	33.8, 23.8, 19.4 ^c	50.3, 50.3, 50.3	49.5 9	37 ⁱ	No
		90	Φ_{h}	40.4, 23.5, 20.3 ^b	46.9, 46.9, -	46.9 f	5 h	
12	(3,4,5)18G1-COORb	170	BCC	33.8, 27.8, 19.4 ^c	47.8, 47.8, 47.8	47.1 <i>9</i>	34 ⁱ	No
		120	Φ_{h}	38.4, 22.3, 19.2 ^b	44.5, 44.5, -	44.5 f	5 h	
13	(3,4,5)18G1-COOK	135	BCC	33.7, 23.8, 19.3 ^c	47.5, 47.5, 47.5	46.8 9	34 ⁱ	No
		100	Φ_{h}	38.7, 22.3, 19.3 ^b	44.6, 44.6, -	44.6 ^f	5 h	
14	(3,4,5)18G1-COONa	135	BCC	31.8, 22.4, 18.3 ^c	44.9, 44.9, 44.9	44.2 9	29 ⁱ	No
		100	Φ_{h}	36.2, 20.8, 18.0 ^b	41.4, 41.1, –	41.1 ^f	5 h	
15	(3,4,5)18G1-COOLi	150	BCC	31.0, 21.8, 17.8 ^c	43.7, 43.7, 43.7	43.0 9	27 i	No
		110	Φ_{h}	33.0, 19.1, 16.5 ^b	38.1, 38.1, –	38.1 ^f	4 ^h	

^a Phase notation: Φ_h –columnar hexagonal phase; **BCC** – body-centered cubic phase; $Pm\bar{3}n$ – cubic phase. ^b Experimental d-spacings for the Φ_h phases. ^c Experimental d-spacings for the **BCC** phase. ^d Experimental d-spacings for the $Pm\bar{3}n$ phase. ^e Lattice parameters calculated using $d_{hk} = (\sqrt{3}a/2) \bullet (h^2 + k^2 + hk)^{-1/2}$ for hexagonal phases, and $d_{hkl} = (a) \bullet (h^2 + k^2 + l^2)^{-1/2}$ for the cubic phase. ^f Column diameter for Φ_h phases $(D_{col} = a)$ and ^g sphere diameter for the **BCC** phase $(D_{sphere} = \sqrt{3}a/2)$; $D_{sph} = 2(3a^3/32\pi)^{1/3}$ for $Pm\bar{3}n$ phase. ^h Number of monodendrons per stratum. ⁱ Number of monodendrons per spherical dendrimer.

phases were also investigated for the SOM effect (right side structures in Fig. 4) [66]. Their detailed analysis is summarized on the top of Table 2, entries 1 to 3. No SOM was detected in any of the 18 assemblies from Fig. 4.

Fig. 5 shows two additional conical conformers self-assembling in supramolecular spheres self-organizing in A15 (*Pm3n*) phases (4–3,4,5–3,5)12G2-CH₂OH [54] in the top left corner of Fig. 5 and (4Pr-(3,4,5Pr)²)12G2-CH₂OH [59] in the bottom left corner of Fig. 5. Their analysis for the SOM effect is summarized in Table 2 entries 4 and 5. No SOM was observed for these compounds either (Figs. S2–S5). Therefore, these 20 experiments indicate that the conical dendrons forming spheres do not favor the SOM effect. Four crown dendrimers, three covalent (Fig. 5c, d, f) and one dynamic supramolecular (Fig. 5e) were investigated for the SOM effect. The SOM effect of compounds c and d were already published and are summarized in Fig. 3 [23,24,68]. The SOM of

the covalent crown compound, (4–3,4,5)12G1-CTTV (Fig. 5f) [69], is the tetramer of compound that is the higher homologue of its covalent crown trimer, 3,4,5–12G1-CTV (Figs. 3 and 5c). The SOM of compound (4Pr-(3,4,5Pr)²)12G2-COOH [69] from Fig. 5e will be discussed in the next subchapter.

The SOM effect of self-assembling covalent crown dendrimer (4–3,4,5)12G1-CTTV

(4–3,4,5)12G1-CTTV (Figs. 5f and 6e) [69] is the corresponding tetramer of the more rigid (3,4,5)12G1-CTV trimer (Fig. 5c). Therefore, the CTTV derivative can be considered as a more dynamic [93] version of the CTV. However, both dendronized compounds exhibit crown conformations.

The oriented fiber XRD of the dendronized CTTV in the A15 $(Pm\bar{3}n)$ phases (Fig. 6a,b) as well as after cooling back to p6mm

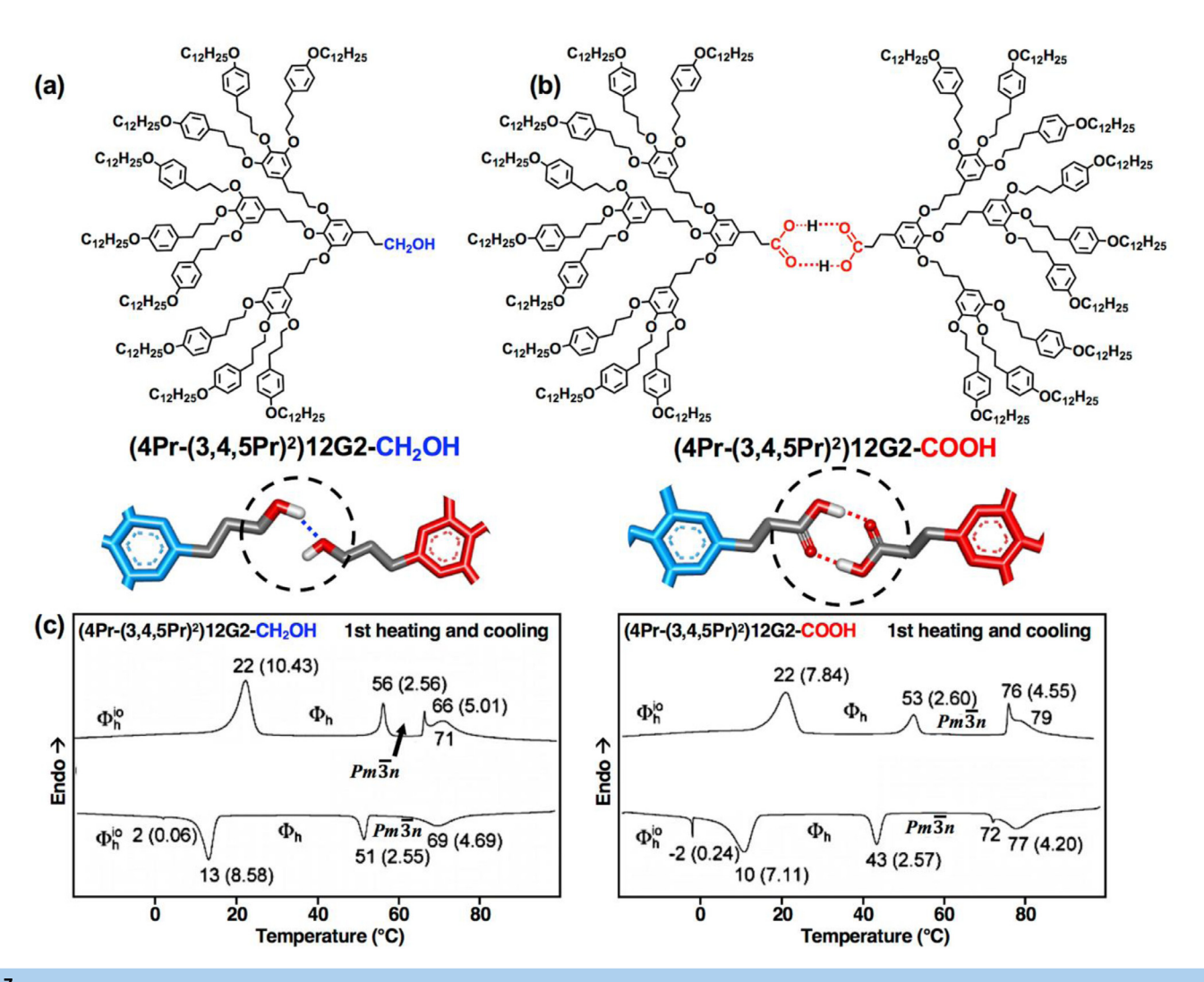


Fig. 7

Chemical structures of self-assembling dendrons (4Pr-(3,4,5Pr)²)12G2-CH₂OH, (4Pr-(3,4,5Pr)²)12G2-COOH and their hydrogen bonding interactions at the apex (a-b). DSC traces of first heating and cooling of the supramolecular assemblies generated from (4Pr-(3,4,5Pr)²)12G2-CH₂OH and (4Pr-(3,4,5Pr)²)12G2-COOH at 10 °C/min (c). Phases indexed by small-angle XRD, transition temperatures (in °C), and associated enthalpy changes (in parentheses in kcal/mol) are presented.

(Fig. 6c, d) are almost identical with the one of the CTV derivative (Fig. 3b). The 4-folded symmetry of the XRD from Fig. 6d, h are explained by the orthogonal arrangement of hexagonal columns that is directed by the close contact spheres from the (200), (020), (002) directions of the A15 phase from Fig. 6i to become the (100), (101) and (001) directions in the orthogonal arrangements of hexagonal columns. The DSC scans showing in Fig. 6j display very sharp and well defined first order transitions both on heating and cooling from *p6mm* to the A15 phase.

A comparison of SOM of $(4Pr-(3,4,5Pr)^2)12G_2$ – CH_2OH and $(4Pr-(3,4,5Pr)^2)12G2$ -COOH

Fig. 7a, b compares the structures of these two dendrons. They differ only by the functional group attached at their apex. Compound $(4Pr-(3,4,5Pr)^2)12G_2-CH_2OH$ (Fig. 7a) contains a -CH₂OH H-bonding group at apex while compound $(4Pr-(3,4,5Pr)^2)12G_2-COOH$ (Fig. 7b) contains a -COOH H-bonding

group at its apex. The ${\text{-CH}_2\text{OH}}$ group can form only one H-bond while the ${\text{-COOH}}$ group forms a double H-bond that usually adopts a hexagonal geometry. See and compare the structures from the bottom of a and b in Fig. 7.

The supramolecular assemblies derived from these two building blocks generate identical assemblies, columnar hexagonal arrays almost within the same range of temperatures followed by an A15 phase at higher temperature. DSC traces of these supramolecular assemblies with their structures assigned by XRD experiments are shown in the left and right sides of Fig. 7c. Therefore, XRD experiments cannot decide if there is a different mechanism responsible for the self-assembly of these two compounds containing different H-bonding groups at its apex. Compound $(4\text{Pr-}(3,4,5\text{Pr})^2)12\text{G2-CH}_2\text{OH}$ from Fig. 7a self-organizes in an A15 $(Pm\bar{3}n)$ phase that does not exhibit a SOM (Table 2, entry 5) while compound b from Fig. 7 displays a SOM effect (Table 2, entry 6).

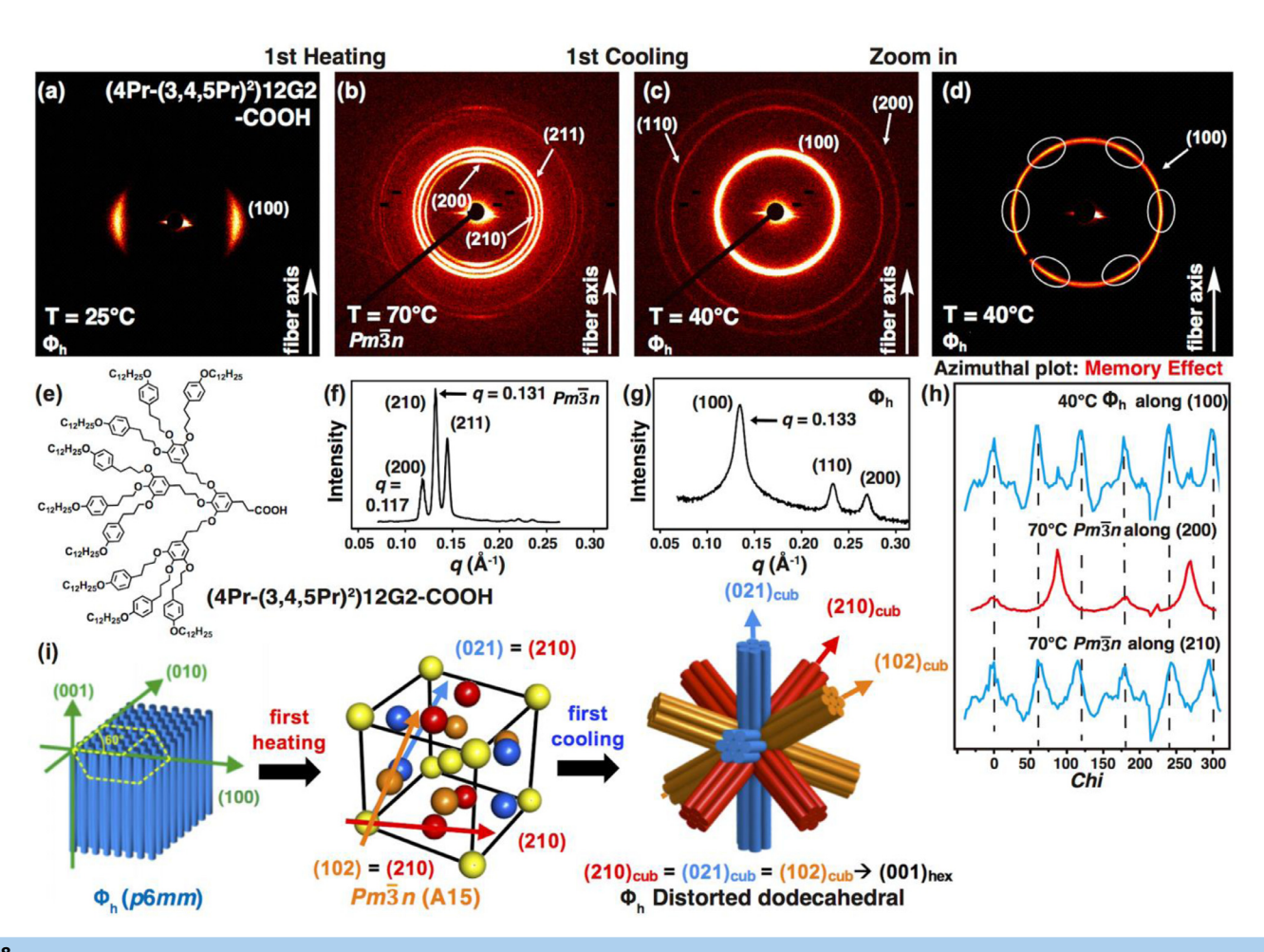


Fig. 8

Structural and retrostructural analysis by small-angle XRD (a-d) of the fiber of the supramolecular assembly generated from the supramolecular crown of (4Pr-(3,4,5Pr)²)12G2-COOH (e) aligned by extrusion at 25 °C, on first heating and cooling. XRD plots of $Pm\bar{3}n$ (A15) and Φ_h (p6mm) lattices (f, g). Azimuthal plots (h) of the patterns in (d) along (100)_{hex}, and the patterns in (b) along (200)_{cub} and (210)_{cub}. Schematic representation of the lattice transition between columnar hexagonal Φ_h (p6mm) and cubic ($Pm\bar{3}n$, A15) lattice on first heating and cooling (i). Supramolecular orientational memory induced by (210)_{cub} of $Pm\bar{3}n$ (A15) to (100)_{hex} results in a distorted dodecahedral architecture generated from columnar hexagonal assemblies of supramolecular columns.

Discriminating between mechanisms of self-organization by SOM

The two self-assembling dendrons shown in Fig. 7 and analyzed in Table 2, entries 4 and 5 self-organize into identical periodic arrays of supramolecular columns and spheres and differ only in the presence of absence of a SOM effect. A statistical analysis of the 20 conical molecules from Figs. 4 and 5 and Tables 1 and 2 demonstrate that conical dendrons forming supramolecular spheres do not display SOM effects. At the same time all 3 self-assembling covalent crowns from Fig. 5 self-organize Frank-Kasper and BCC phases that display SOM (Table 2). Therefore, compound b from Fig. 7 exhibits a dynamic supramolecular crown conformation while compound a from Fig. 7 exhibit a conical conformation. The stronger and more directional H-bonding between the two -COOH groups is responsible for the assembly of the dynamic supramolecular crown conformation of compound b from Fig. 7. The next question to be addressed is the following: Is a dynamic supramolecular crown forming a supramolecular sphere exhibiting the same or a different SOM from the one generated by covalent crown?

Discovery of a novel SOM mediated by self-assembling dynamic supramolecular crowns

The analysis of the SOM of (4Pr-(3,4,5Pr)2)12G2-COOH by the method discussed previously in Figs. 3 and 6 is shown in Fig. 8.

Fig. 8e shows the structure of this compound. Its oriented fiber XRD are presented in Fig. 8a–h. The most interesting and unexpected result is that Fig. 8d and h demonstrate a complex symmetry rather than the 4-fold symmetry observed previously in Figs. 3b,d and 6d,i upon cooling an oriented fiber from the A15 phase back to the *p6mm* columnar hexagonal phase. This simply means that the orthogonal arrangements of hexagonal columns obtained previously by SOM with covalent crown constructed supramolecular spheres was replaced by a distorted dodecahedral arrangement of hexagonal arrangements of columns (Figs. 8i, S6 and S7). This new supramolecular architecture and morphology is unprecedented and can be constructed only *via* the SOM mechanism reported here.

This new morphology also demonstrates that the distorted dodecahedral arrangement of hexagonal columns is not mediated by the close contact spheres from the (200), (020) and (002)

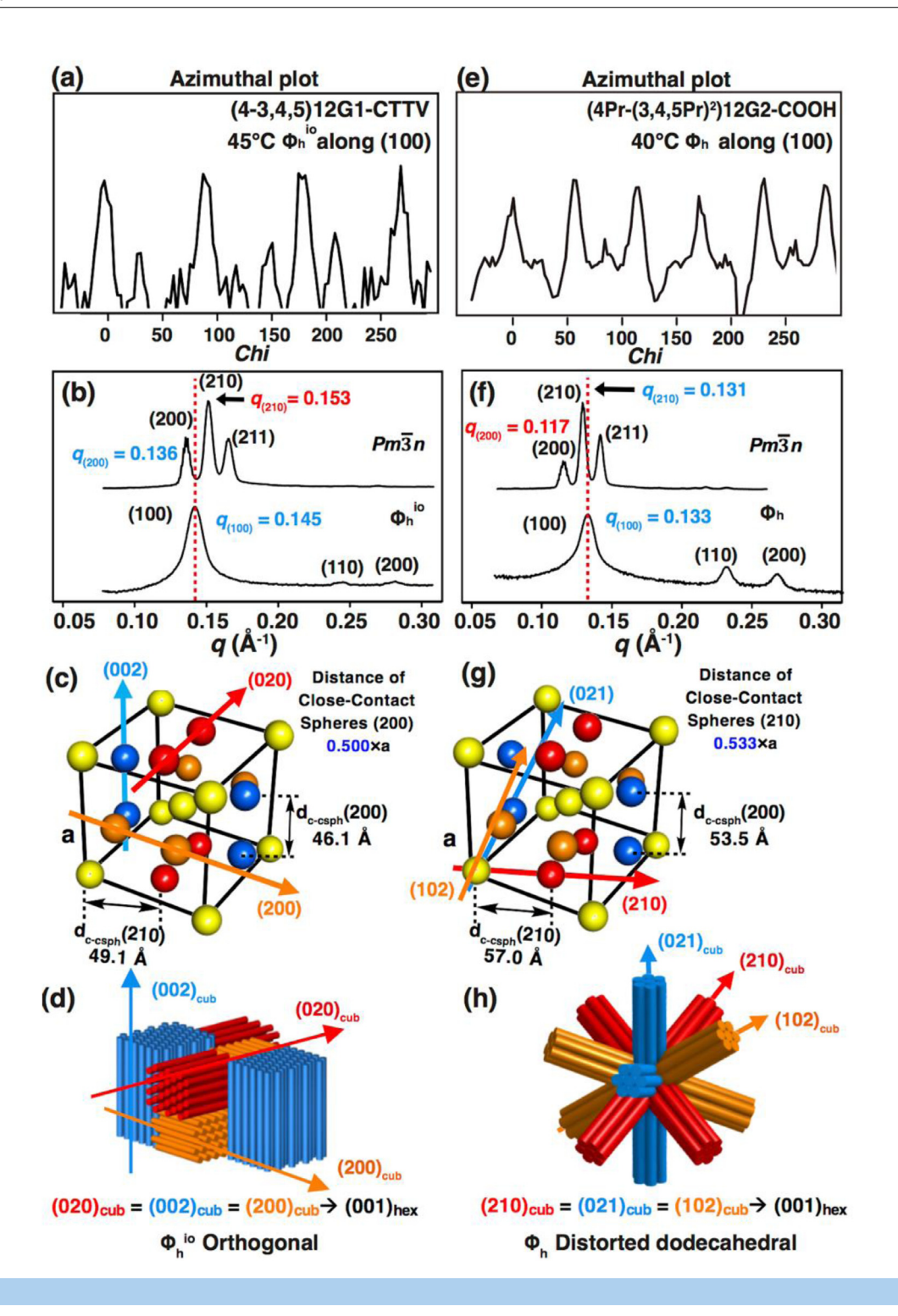


Fig. 9

Comparison between two different supramolecular orientational memory (SOM) effects by the same lattice symmetry, A15 to the columnar hexagonal array. Azimuthal plots of small-angle XRD of (4-3,4,5)12G1-CTTV along $(100)_{hex}$ (a), its close-contact distance of spheres along (200) (b), and its orthogonal architecture mediated by SOM (c). d_{c-csph} is the distance between two close-contact spheres along the designated axis. Azimuthal plots of XRD of $(4Pr-(3,4,5Pr)^2)12G2$ -COOH along $(100)_{hex}$ (d), its close-contact distance of spheres along (210) (e), and its distorted dodecahedral architecture mediated by SOM (f).

directions of the A15 phase but by the close contact spheres from the (210), (021) and (102) directions of the A15 Frank-Kasper phase (Fig. 8i).

The close contact distances between the spheres arranged on the (200) direction of the A15 phase of the dynamic

supramolecular crown is $d_{c-csph} = 53.5$ A while the distance for the close contact spheres on the (210) direction is $d_{c-csph} = 57.0$ A (Fig. 9g). The same values for the SOM mediated by (4–3,4,5)12G1CTTV that provides an orthogonal arrangement of hexagonal spheres are shown in Fig. 9c. Fig. 9f seems to indicate

Table 2
Structural Analysis of Conical and Crown-Like Conformations of Self-Assembling Dendrons and Dendrimers by Small-Angle XRD to Search for the Orientational Memory Effect.

No	Molecule	T (°C)	Phase ^a	$d_{100}, d_{110}, d_{200}$ $(\mathring{A})^b$ $d_{110}, d_{200}, d_{211}$ $(\mathring{A})^c$ $d_{11}, d_{20}, d_{02} (\mathring{A})^d$ $d_{200}, d_{210}, d_{211}$ $(\mathring{A})^e$	a, b, c (Å) ^g	D _{col} ^h / D _{sph} ⁱ (Å)	μ	Memory Effect
1	(4BpPr-3,4BpPr- 3,5BpPr)12G2-COOCH ₃	185	Pm3̄n	138.1, 122.2, 113.6 ^e	276.0, 276.0, 276.0	171.2 ⁱ	771	No
		135	Φ_{r-c}	112.0, 82.0, 74.4 ^d	163.2, 149.2, –	_	17	
		110	Lam ^k	71.8, 35.9, 23.9 ^f	71.8, –, –	71.8	-	
2	(3,4BpPr) ² 12G2-COOCH ₃	115	Pm3n	84.4, 75.4, 69.0 ^e	168.8, 168.8, 168.8	104.7 ′	267	No
		75	Φ_{r-c}	82.7, 72.9, 49.8 ^d	145.6, 99.5, –	_	15	
3	(3,4BpPr) ² 12G2-CH ₂ OH	140	Pm3̄n	77.5, 69.7, 63.6 ^e	155.5, 155.5, 155.5	96.5 ⁱ	213	No
		20	Φ_{r-c}	85.4, 65.7, – ^d	131.3, 112.0, –	-	16	
4	(4-3,4,5-3,5)12G2-CH ₂ OH	90	Pm3̄n	43.7, 39.1, 35.6 ^e	87.3, 87.3, 87.3	54.2 ′	25	No
		70	Φ_{h}	40.7, 23.4, 20.2 ^b	46.7, 46.7, -	46.7 h	3	
5	(4Pr-(3,4,5Pr) ²)-12G2-	65	Pm3̄n	55.0, 49.1, 44.8 ^e	109.8, 109.8, 109.8	68.1 <i>i</i>	29	No
	CH₂OH	25	Φ_{h}	46.1, 26.6, 23.0 ^b	53.2, 53.2, -	53.2 h	2	
6	(4Pr-(3,4,5Pr) ²)-12G2-	60	Pm3̄n	53.4, 47.8, 43.6 ^e	106.9, 106.9, 106.9	66.3 ⁱ	30	Yes
	СООН	30	Φ_{h}	47.4, 27.2, 23.6 ^b	54.5, 54.5 -	54.5 h	2	
7	(3,4Pr-3,4,5)12G2-0-PBI	180	BCC	38.4, 25.9, 21.1 ^c	51.6, 51.6, 51.6	44.7 ⁱ	12	Yes
		80	$\Phi_{h}{}^{io}$	42.9, –, 21.5 ^b	49.5, 49.5, -	49.5 ^h	2	
		0	$\Phi_{h}{}^{k}$	42.5, 24.5, 21.2 ^b	48.8, 48.8, 19.2	48.8 h	2	
8	(3,4,5)12G1-CTV	80	Pm3̄n	36.6, 32.7, 29.8 ^e	73.5, 73.5, 73.5	45.6 ⁱ	7	Yes
		65	$\Phi_{h}{}^{io}$	35.6, 20.5, 17.8 ^b	41.1, 41.1, –	41.1 ^h	1	
9	(4-3,4,5)12G1-CTTV	125	Pm3̄n	46.1, 41.2, 37.6 ^e	92.2, 92.2, 92.2	57.2 ⁱ	7	Yes
		25	Φ_{h}	43.4, 25.0, 21.7 ^b	50.1, 50.1, -	50.1 ^h	1	

^a Phase notation: $\Phi_{\mathbf{h}}$ –columnar hexagonal phase; $\Phi_{\mathbf{rc}}$ –centered rectangular columnar phase; \mathbf{BCC} –body-centered cubic phase; $Pm\bar{3}n$ – cubic phase; \mathbf{Lam} – Lamellar phase. ^b Experimental d-spacings for the $\Phi_{\mathbf{h}}$ phases. ^c Experimental d-spacings for the \mathbf{BCC} phase. ^g Experimental d-spacings for the $\Phi_{\mathbf{rc}}$ phase. ^g Conly observed only in the first heating of the as prepared compound. ^g Lattice parameters calculated using $d_{hk} = (\sqrt{3}a/2) \cdot (h^2 + k^2 + hk)^{-1/2}$ for the equation of the phases, and $d_{hk} = (a) \cdot (h^2 + k^2 + l^2)^{-1/2}$ for the cubic phase. ^h Column diameter for $\Phi_{\mathbf{h}}$ phases ($D_{\text{col}} = a$) and ^j sphere diameter for the **BCC** phase ($D_{\text{sphere}} = \sqrt{3}a/2$); $D_{\text{sph}} = 2(3a^3/32\pi)^{1/3}$ for $Pm\bar{3}n$ phase.

that for the self-organization and SOM process of the dynamic supramolecular crown the (210) direction of the A15 corresponds most closely with the (100) direction of its columnar hexagonal phase while for the covalent crown (4–3,4,5)12G1-CTTV the (100) direction of the columnar hexagonal phase is closer to the (200) direction of its A15 phase (Fig. 9b). It should be mentioned that the previously published orthogonal SOM on (3,4,5)12G1-CTV [23] showed similar correlation between (100) direction of the hexagonal phase and (200) direction of its A15 to Fig. 9b. This mechanism must be supported by other examples of SOM mediated by spherical assemblies generated from dynamic supramolecular crowns.

Why are crown conformers assembling spheres dominating the SOM process?

Fig. 10 provides a hypothesis for the explanation of these results. The bottom part of Fig. 10 shows the number of steps involved during the transition from a chiral racemic or homochiral supramolecular sphere assembled from conical dendrons.

When the column contains tilted dendrons and therefore is helical racemic or homochiral [66,94,95] there are 5 steps involved

in this process. Since the conical dendron is quasiequivalent, just like the proteins in viruses [72] it can undergo a first transition from cone to taper, to tilted taper to a cross-section of the column and to column. When the column containing non-tilted dendrons there are only 4 steps involved in this process (see second set of data from the bottom part of Fig. 10). However, both covalent and dynamic supramolecular crowns can undergo inversion of configuration and therefore the transition from a supramolecular sphere to a supramolecular column requires only one step (middle part of Fig. 10). Irrespective of whether these mechanisms are concerted or stepwise, the crown conformer-based sphere most probably is favoring the SOM process. The upper part of Fig. 10 summarizes the hierarchical transition from the columnar hexagonal arrays to the orthogonal and tetrahedral arrangements of hexagonal columns via the A15 and BCC phases respectively. The mechanism of self-assembly of helical supramolecular dendrimers [46,94,96–105] and self-organized dendronized polymers is more advanced than that of the corresponding supramolecular spheres and the experiments reported here make a substantial step ahead towards access to the mechanism of self-assembly of supramolecular spheres and of their periodic arrays.

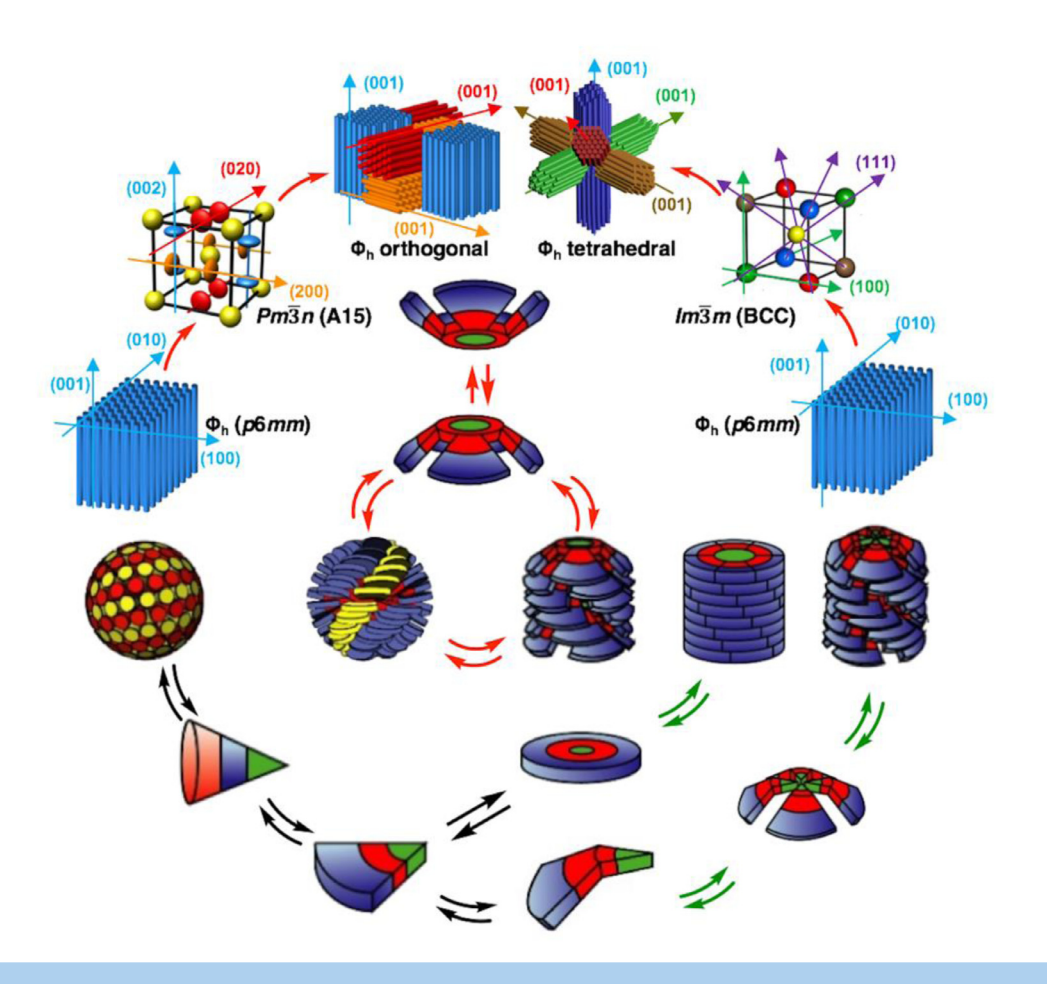


Fig. 10

The hierarchical mechanisms of interconversion between supramolecular spheres and columns that facilitates the supramolecular orientational memory effect that generates complex architectures assembled from hexagonal arrays of supramolecular columns.

Conclusions

A statistical analysis of the SOM process of a library of 20 supramolecular spheres assembled from self-assembling conical shape dendrons and of a library of 4 supramolecular spheres assembled 3 covalent crowns and one from a dynamic adaptive supramolecular self-assembling crown demonstrated that both covalent and dynamic supramolecular self-assembling crowns dictate the supramolecular orientational memory (SOM) process. A one step, most probably concerted transition from supramolecular spheres to supramolecular columns and the reverse process involves a single step inversion of crown configuration and is most probably the reason for this result. By contrast the transition from supramolecular spheres generated from conical dendrons to supramolecular columns and the reverse process involves 5 or 4 concerted or stepwise steps that ultimately favor the crown conformer as the one that dictates the SOM process. The SOM effect of the dynamic supramolecular crown provided an unprecedented distorted dodecahedral architecture of hexagonal arrangements of columns that cannot be accomplished via any other methodology except the SOM reported here. We expect that this SOM concept will be able to engineer numerous new complex arrangements of columns arranged in a hexagonal or other periodic array. More experiments and theoretical work are needed to demonstrate the universality of this process.

Declaration of Competing Interest

The authors declare that they have no known competing financial interests or personal relationships that could have appeared to influence the work reported in this paper.

Acknowledgement

This work was supported by National Science Foundation Grants DMR-1066116, DMR-1807127 and DMR-1720530, the P. Roy Vagelos Chair at the University of Pennsylvania (all to V.P.). B.E.P. thanks the Howard Hughes Medical Institute for an International Student Research Fellowship. The authors thank Professor P. A. Heiney from University of Pennsylvania for discussions of the XRD analysis. The authors acknowledge use of the Dual Source and Environmental X-ray Scattering facility operated by the Laboratory for Research on the Structure of Matter at the University of Pennsylvania (NSF MRSEC 17-20530). The equipment purchase was made possible by a NSF MRI grant (17-25969), a ARO DURIP grant (W911NF-17-1-0282), and the University of Pennsylvania.

Author contributions

V.P. designed the project and guided all the experiments; N.H., M.P., and B.E.P. performed the fiber XRD, M.R.I., M.J.S., M.N.H, D.A.W, and B.M.R synthesized molecules, N.H., M.P., B.E.P, Q.X.

and V.P analyzed the data, and N.H., B.E.P., Q.X., and V.P. prepared the figures and wrote the paper.

Supplementary materials

Supplementary material associated with this article can be found, in the online version, at doi:10.1016/j.giant.2020.100001.

References

- [1] S.B. Prusiner, Novel proteinaceous infectious particles cause scrapie, Science 216 (1982) 136–144. doi:10.1126/science.6801762.
- [2] S.B. Prusiner, Molecular biology of prion diseases, Science 252 (1991) 1515– 1522, doi:10.1126/science.1675487.
- [3] K.M. Pan, M. Baldwin, J. Nguyen, M. Gasset, A. Serban, D. Groth, I. Mehlhorn, Z. Huang, R.J. Fletterick, F.E. Cohen, Conversion of alpha-helices into betasheets features in the formation of the scrapie prion proteins, Proc. Natl. Acad. Sci. USA 90 (1993) 10962–10966, doi:10.1073/pnas.90.23.10962.
- [4] S.B. Prusiner, Prions, Proc. Natl. Acad. Sci. USA 95 (1998) 13363–13383, doi:10. 1073/pnas.95.23.13363.
- [5] J. King, C. Haase-Pettingell, D. Gossard, Protein folding and misfolding: the exquisite three-dimensional structures of proteins allow their diverse functions, but exactly how proteins fold remains a puzzle, Am. Sci. 90 (2002) 445–453.
- [6] E.T. Powers, D.L. Powers, Mechanisms of protein fibril formation: nucleated polymerization with competing off-pathway aggregation, Biophys. J. 94 (2008) 379–391, doi:10.1529/biophysj.107.117168.
- [7] A. Ölander, An electrochemical investigation of solid cadmium-gold alloys, J. Am. Chem. Soc. 54 (1932) 3819–3833, doi:10.1021/ja01349a004.
- [8] K.E. Schurch, K.H.G. Ashbee, A near perfect shape-memory ceramic material, Nature 266 (1977) 706–707, doi:10.1038/266706a0.
- [9] M.V. Swain, Shape memory behaviour in partially stabilized zirconia ceramics, Nature 322 (1986) 234–236, doi:10.1038/322234a0.
- [10] H.-R. Wenk, P. Kaercher, W. Kanitpanyacharoen, E. Zepeda-Alarcon, Y. Wang, Orientation relations during the α ω phase transition of zirconium: in situ texture observations at high pressure and temperature, Phys. Rev. Lett. 111 (2013) 195701, doi:10.1103/PhysRevLett.111.195701.
- [11] A. Lai, Z. Du, C.L. Gan, C.A. Schuh, Shape memory and superelastic ceramics at small scales, Science 341 (2013) 1505–1508, doi:10.1126/science.1239745.
- [12] A. Lendlein, H. Jiang, O. Jünger, R. Langer, Light-induced shape-memory polymers, Nature 434 (2005) 879–882, doi:10.1038/nature03496.
- [13] T. Xie, Tunable polymer multi-shape memory effect, Nature 464 (2010) 267–270, doi:10.1038/nature08863.
- [14] A.A. Shah, B. Schultz, W. Zhang, S.C. Glotzer, M.J. Solomon, Actuation of shapememory colloidal fibres of Janus ellipsoids, Nat. Mater. 14 (2015) 117–124, doi:10.1038/nmat4111.
- [15] A. Lendlein, R. Langer, Biodegradable, elastic shape-memory polymers for potential biomedical applications, Science 296 (2002) 1673–1676, doi:10.1126/ science.1066102.
- [16] I. Dozov, M. Nobili, G. Durand, Fast bistable nematic display using monostable surface switching, Appl. Phys. Lett. 70 (1997) 1179–1181, doi:10.1063/1.118479.
- [17] T. Araki, M. Buscaglia, T. Bellini, H. Tanaka, Memory and topological frustration in nematic liquid crystals confined in porous materials, Nat. Mat. 10 (2011) 303– 309, doi:10.1038/nmat2982.
- [18] F. Serra, M. Buscaglia, T. Bellini, The emergence of memory in liquid crystals, Mater. Today 14 (2011) 488–494, doi:10.1016/S1369-7021(11)70213-9.
- [19] W. Sokolowski, A. Metcalfe, S. Hayashi, L. Yahia, J. Raymond, Medical applications of shape memory polymers, Biomed. Mater 2 (2007) S23–S27, doi:10.1088/1748-6041/2/1/S04.
- [20] Y. Furusho, T. Kimura, Y. Mizuno, T. Aida, Chirality-memory molecule: a D₂-symmetric fully substituted porphyrin as a conceptually new chirality sensor, J. Am. Chem. Soc. 119 (1997) 5267–5268, doi:10.1021/ja970431q.
- [21] E. Yashima, K. Maeda, Y. Okamoto, Memory of macromolecular helicity assisted by interaction with achiral small molecules, Nature 399 (1999) 449–451, doi:10. 1038/20900.
- [22] F. Helmich, M.M.J. Smulders, C.C. Lee, A.P.H.J. Schenning, E.W. Meijer, Effect of stereogenic centers on the self-sorting, depolymerization, and atropisomerization kinetics of porphyrin-based aggregates, J. Am. Chem. Soc. 133 (2011) 12238–12246, doi:10.1021/ja204543f.
- [23] M. Peterca, M.R. Imam, S.D. Hudson, B.E. Partridge, D. Sahoo, P.A. Heiney, M.L. Klein, V. Percec, Complex arrangement of orthogonal nanoscale columns via a supramolecular orientational memory effect, ACS Nano 10 (2016) 10480– 10488, doi:10.1021/acsnano.6b06419.
- [24] D. Sahoo, M. Peterca, E. Aqad, B.E. Partridge, P.A. Heiney, R. Graf, H.W. Spiess, X. Zeng, V. Percec, Tetrahedral arrangements of perylene bisimide columns via supramolecular orientational memory, ACS Nano 11 (2017) 983–991, doi:10. 1021/acsnano.6b07599.
- $\hbox{[25] D. Sahoo, M. Peterca, E. Aqad, B.E. Partridge, M.L. Klein, V. Percec, Losing supramolecular orientational memory {\it via} self-organization of a } \\$

- misfolded secondary structure, Polym. Chem. 9 (2018) 2370–2381, doi:10.1039/C8PY00187A.
- [26] B.M. Rosen, C.J. Wilson, D.A. Wilson, M. Peterca, M.R. Imam, V. Percec, Dendron-mediated self-assembly, disassembly, and self-organization of complex systems, Chem. Rev. 109 (2009) 6275–6540, doi:10.1021/cr900157q.
- [27] H.-J. Sun, S. Zhang, V. Percec, From structure to function via complex supramolecular dendrimer systems, Chem. Soc. Rev. 44 (2015) 3900–3923, doi:10.1039/C4CS00249K.
- [28] V. Percec, Merging macromolecular and supramolecular chemistry into bioinspired synthesis of complex systems, Isr. J. Chem. 60 (2020) 48–66, doi:10. 1002/ijch.202000004.
- [29] F.C. Frank, J.S. Kasper, Complex alloy structures regarded as sphere packings. I. Definitions and basic principles, Acta Cryst 11 (1958) 184–190, doi:10.1107/ S0365110X58000487.
- [30] F.C. Frank, J.S. Kasper, Complex alloy structures regarded as sphere packings. II. Analysis and classification of representative structures, Acta Cryst. 12 (1959) 483–499, doi:10.1107/S0365110X59001499.
- [31] A.F. Schuch, R.L. Mills, Crystal structures of the three modifications of nitrogen 14 and nitrogen 15 at high pressure, J. Chem. Phys. 52 (1970) 6000–6008, doi:10. 1063/1.1672899.
- [32] D.T. Cromer, R.L. Mills, D. Schiferi, L.A. Schwalbe, The structure of N_2 at 49 kbar and 299K, Acta Cryst. B 37 (1981) 8–11, doi:10.1107/S0567740881002070.
- [33] S. Nosé, M.L. Klein, Structural transformations in solid nitrogen at high pressure, Phys. Rev. Lett. 50 (1983) 1207–1210, doi:10.1103/PhysRevLett.50.1207.
- [34] S. Buchsbaum, R.L. Mills, D. Schiferl, Phase diagram of nitrogen determined by Raman spectroscopy from 15 to 300K at pressures to 52GPa, J. Phys. Chem. 88 (1984) 2522–2525, doi:10.1021/j150656a018.
- [35] R.L. Mills, B. Olinger, D.T. Cromer, Structures and phase diagrams of N2 and Co to 13GPa by x-ray diffraction, J. Chem. Phys. 84 (1986) 2837–2845, doi:10. 1063/1.450310.
- [36] D. Tomasino, Z. Jenei, W. Evans, C.-S. Yoo, Melting and phase transitions of nitrogen under high pressures and temperatures, J. Chem. Phys. 140 (2014) 244510, doi:10.1063/1.4885724.
- [37] R.L. Mills, B. Olinger, D.T. Cromer, Structures and phase diagrams of N_2 and CO to 13GPa by x-ray diffraction, J. Chem. Phys. 84 (1986) 2837–2845, doi:10.1063/1.450310.
- [38] M.L. Klein, D. Levesque, J.-J. Weis, Molecular-dynamics study of solid γ -O₂, Phys. Rev. B 21 (1980) 5785–5792, doi:10.1103/PhysRevB.21.5785.
- [39] B.J. Baer, Malcolm. Nicol, high-pressure binary phase diagram of nitrogenoxygen at 295K determined by Raman spectroscopy, J. Phys. Chem. 94 (1990) 1073–1078, doi:10.1021/j100366a009.
- [40] D. Sihachakr, P. Loubeyre, O_2 / N_2 mixtures under pressure: a structural study of the binary phase diagram at 295K, Phys. Rev. B 70 (2004) 134105, doi:10.1103/PhysRevB.70.134105.
- [41] Y. Akahama, T. Maekawa, T. Sugimoto, H. Fujihisa, N. Hirao, Y. Ohishi, High-pressure phase diagram of O_2 and N_2 binary system: formation of Kagome-Lattice of O_2 , J. Phys. Conf. Ser. 500 (2014) 182001, doi:10.1088/1742-6596/500/18/182001.
- [42] P. Mariani, V. Luzzati, H. Delacroix, Cubic phases of lipid-containing systems: structure analysis and biological implications, J. Mol. Biol. 204 (1988) 165–189, doi:10.1016/0022-2836(88)90607-9.
- [43] P. Sakya, J.M. Seddon, R.H. Templer, R.J. Mirkin, G.J.T. Tiddy, Micellar cubic phases and their structural relationships: the nonionic surfactant system C₁₂EO₁₂/Water, Langmuir 13 (1997) 3706–3714, doi:10.1021/la9701844.
- [44] V.S.K. Balagurusamy, G. Ungar, V. Percec, G. Johansson, Rational design of the first spherical supramolecular dendrimers self-organized in a novel thermotropic cubic liquid-crystalline phase and the determination of their shape by X-ray analysis, J. Am. Chem. Soc. 119 (1997) 1539–1555, doi:10.1021/ja963295i.
- [45] S.D. Hudson, H.-T. Jung, V. Percec, W.-D. Cho, G. Johansson, G. Ungar, V.S.K. Balagurusamy, Direct visualization of individual cylindrical and spherical supramolecular dendrimers, Science 278 (1997) 449–452, doi:10.1126/science. 278.5337.449.
- [46] V. Percec, C.-H. Ahn, G. Ungar, D.J.P. Yeardley, M. Möller, S.S. Sheiko, Controlling polymer shape through the self-assembly of dendritic side-groups, Nature 391 (1998) 161–164, doi:10.1038/34384.
- [47] V. Percec, W.-D. Cho, P.E. Mosier, G. Ungar, D.J.P. Yeardley, Structural analysis of cylindrical and spherical supramolecular dendrimers quantifies the concept of monodendron shape control by generation number, J. Am. Chem. Soc. 120 (1998) 11061–11070, doi:10.1021/ja9819007.
- [48] V. Percec, W.-D. Cho, M. Möller, S.A. Prokhorova, G. Ungar, D.J.P. Yeardley, Design and structural analysis of the first spherical monodendron selforganizable in a cubic lattice, J. Am. Chem. Soc. 122 (2000) 4249–4250, doi:10. 1021/ja9943400.
- [49] V. Percec, W.-D. Cho, G. Ungar, Increasing the diameter of cylindrical and spherical supramolecular dendrimers by decreasing the solid angle of their monodendrons via periphery functionalization, J. Am. Chem. Soc. 122 (2000) 10273–10281, doi:10.1021/ja0024643.
- [50] D.J.P. Yeardley, G. Ungar, V. Percec, M.N. Holerca, G. Johansson, Spherical supramolecular minidendrimers self-organized in an "inverse micellar"-like

- thermotropic body-centered cubic liquid crystalline phase, J. Am. Chem. Soc. 122 (2000) 1684–1689, doi:10.1021/ja993915q.
- [51] V. Percec, W.D. Cho, G. Ungar, D.J.P. Yeardley, From molecular flat tapers, discs, and cones to supramolecular cylinders and spheres using Frechet-type monodendrons modified on their periphery, Angew. Chem. Int. Ed. 39 (2000) 1597–1602, doi:10.1002/(SICI)1521-3773(20000502). 39:9<1597::AID-ANIE1597>3.0.CO:2-1
- [52] G. Ungar, V. Percec, M.N. Holerca, G. Johansson, J.A. Heck, Heat-shrinking spherical and columnar supramolecular dendrimers: their interconversion and dependence of their shape on molecular taper angle, Chem. Eur. J. 6 (2000) 1258–1266, doi:10.1002/(SICI)1521-3765(20000403). 6:7<1258::AID-CHEM1258>3.0.CO;2-O
- [53] H. Duan, S.D. Hudson, G. Ungar, M.N. Holerca, V. Percec, Definitive support by transmission electron microscopy, electron diffraction and electron density calculations for the formation of a BCC lattice from poly[N-[3,4,5-tris(ndodecan-1-yloxy)benzoyl]ethyleneimine], Chem. Eur. J. 7 (2001) 4134–4141, doi:10.1002/1521-3765(20011001). 7:19<4134::AID-CHEM4134>3.0,CO;2-W
- [54] V. Percec, W.-D. Cho, G. Ungar, D.J.P. Yeardley, Synthesis and structural analysis of two constitutional isomeric libraries of AB₂-based monodendrons and supramolecular dendrimers, J. Am. Chem. Soc. 123 (2001) 1302–1315, doi:10.1021/ja0037771.
- [55] V. Percec, M.N. Holerca, S. Uchida, W.-D. Cho, G. Ungar, Y. Lee, D.J.P. Yeardley, Exploring and expanding the 3-D structural diversity of supramolecular dendrimers with the aid of libraries of alkali metals of their AB₃ minidendritic carboxylates, Chem. Eur. J. 8 (2002) 1106–1117, doi:10.1002/1521-3765(20020301). 8:5<1106::AID-CHEM1106>3.0.CO;2-G
- [56] V. Percec, W.-D. Cho, G. Ungar, D.J.P. Yeardley, Synthesis and NaOTf mediated self-assembly of monodendritic crown ethers, Chem. Eur. J. 8 (2002) 2011–2025, doi:10.1002/1521-3765(20020503). 8:9<2011::AID-CHEM2011>3.0.CO;2-3
- [57] V. Percec, M. Glodde, G. Johansson, V.S.K. Balagurusamy, P.A. Heiney, Transformation of a spherical supramolecular dendrimer into a pyramidal columnar supramolecular dendrimer mediated by the fluorophobic effect, Angew. Chem. Int. Ed. 42 (2003) 4338–4342, doi:10.1002/anie.200351804.
- [58] V. Percec, C.M. Mitchell, W.-D. Cho, S. Uchida, M. Glodde, G. Ungar, X. Zeng, Y. Liu, V.S.K. Balagurusamy, P.A. Heiney, Designing libraries of first generation AB₃ and AB₂ self-assembling dendrons via the primary structure generated from combinations of (AB)_y-AB₃ and (AB)_y-AB₂ building blocks, J. Am. Chem. Soc. 126 (2004) 6078–6094, doi:10.1021/ja049846j.
- [59] V. Percec, M. Peterca, M.J. Sienkowska, M.A. Ilies, E. Aqad, J. Smidrkal, P.A. Heiney, Synthesis and retrostructural analysis of libraries of AB₃ and constitutional isomeric AB₂ phenylpropyl ether-based supramolecular dendrimers, J. Am. Chem. Soc. 128 (2006) 3324–3334, doi:10.1021/ja060062a.
- [60] V. Percec, M.N. Holerca, S. Nununelin, J.L. Morrison, M. Glodde, J. Smidrkal, M. Peterca, B.M. Rosen, S. Uchida, V.S.K. Balagurusamy, M.L. Sienkowska, P.A. Heiney, Exploring and expanding the structural diversity of self-assembling dendrons through combinations of AB, constitutional isomeric AB₂, and AB₃ biphenyl-4-methyl ether building blocks, Chem. Eur. J. 12 (2006) 6216–6241, doi:10.1002/chem.200600178.
- [61] V. Percec, B.C. Won, M. Peterca, P.A. Heiney, Expanding the structural diversity of self-assembling dendrons and supramolecular dendrimers via complex building blocks, J. Am. Chem. Soc. 129 (2007) 11265–11278, doi:10.1021/ja073714j.
- [62] V. Percec, M. Peterca, A.E. Dulcey, M.R. Imam, S.D. Hudson, S. Nummelin, P. Adelman, P.A. Heiney, Hollow spherical supramolecular dendrimers, J. Am. Chem. Soc. 130 (2008) 13079–13094, doi:10.1021/ja8034703.
- [63] V. Percec, M.R. Imam, M. Peterca, D.A. Wilson, P.A. Heiney, Self-assembly of dendritic crowns into chiral supramolecular spheres, J. Am. Chem. Soc. 131 (2009) 1294–1304, doi:10.1021/ja8087778.
- [64] V. Percec, M.R. Imam, M. Peterca, D.A. Wilson, R. Graf, H.W. Spiess, V.S.K. Balagurusamy, P.A. Heiney, Self-assembly of dendronized triphenylenes into helical pyramidal columns and chiral spheres, J. Am. Chem. Soc. 131 (2009) 7662–7677, doi:10.1021/ja8094944.
- [65] M.R. Imam, M. Peterca, U. Edlund, V.S.K. Balagurusamy, V. Percec, Dendronized supramolecular polymers self-assembled from dendritic ionic liquids, J. Polym. Sci. Part A Pol. Chem. 47 (2009) 4165–4193, doi:10.1002/pola.23523.
- [66] B.M. Rosen, D.A. Wilson, C.J. Wilson, M. Peterca, B.C. Won, C. Huang, L.R. Lipski, X. Zeng, G. Ungar, P.A. Heiney, V. Percec, Predicting the structure of supramolecular dendrimers via the analysis of libraries of AB₃ and constitutional isomeric AB₂ biphenylpropyl ether self-assembling dendrons, J. Am. Chem. Soc. 131 (2009) 17500–17521. doi:10.1021/ia907882n.
- [67] V. Percec, M. Peterca, Y. Tsuda, B.M. Rosen, S. Uchida, M.R. Imam, G. Ungar, P.A. Heiney, Elucidating the structure of the Pm3n cubic phase of supramolecular dendrimers through the modification of their aliphatic to aromatic volume ratio, Chem. Eur. J. 15 (2009) 8994–9004, doi:10.1002/chem.200901324.
- [68] D. Sahoo, M. Peterca, E. Aqad, B.E. Partridge, P.A. Heiney, R. Graf, H.W. Spiess, X. Zeng, V. Percec, Hierarchical self-organization of perylene bisimides into supramolecular spheres and periodic arrays thereof, J. Am. Chem. Soc. 138 (2016) 14798–14807, doi:10.1021/jacs.6b09986.
- [69] D. Sahoo, M.R. Imam, M. Peterca, B.E. Partridge, D.A. Wilson, X. Zeng, G. Ungar, P.A. Heiney, V. Percec, Hierarchical self-organization of chiral columns from

- chiral supramolecular spheres, J. Am. Chem. Soc. 140 (2018) 13478–13487, doi:10.1021/jacs.8b09174.
- [70] M.N. Holerca, D. Sahoo, B.E. Partridge, M. Peterca, X. Zeng, G. Ungar, V. Percec, Dendronized poly(2-oxazoline) displays within only five monomer repeat units liquid quasicrystal, A15 and σ Frank-Kasper phases, J. Am. Chem. Soc. 140 (2018) 16941–16947, doi:10.1021/jacs.8b11103.
- [71] D.A. Wilson, K.A. Andreopoulou, M. Peterca, P. Leowanawat, D. Sahoo, B.E. Partridge, Q. Xiao, N. Huang, P.A. Heiney, V. Percec, Supramolecular spheres self-assembled from conical dendrons are chiral, J. Am. Chem. Soc. 141 (2019) 6162–6166, doi:10.1021/jacs.9b02206.
- [72] A. Klug, From macromolecules to biological assemblies (Nobel lecture), Angew. Chem. Int. Ed. Engl. 22 (1983) 565–582, doi:10.1002/anie.198305653.
- [73] V. Percec, Bioinspired supramolecular liquid crystals, Philos. Trans. A Math. Phys. Eng. Sci. 364 (2006) 2709–2719, doi:10.1098/rsta.2006.1848.
- [74] Y. Li, S.-T. Lin, W.A. Goddard, Efficiency of various lattices from hard ball to soft ball: theoretical study of thermodynamic properties of dendrimer liquid crystal from atomistic simulation, J. Am. Chem. Soc. 126 (2004) 1872–1885, doi:10.1021/ja038617e.
- [75] P. Ziherl, R.D. Kamien, From lumps to lattices: crystallized clusters made simple, J. Phys. Chem. B 115 (2011) 7200–7205, doi:10.1021/jp109330p.
- [76] C.R. Iacovella, A.S. Keys, S.C. Glotzer, Self-assembly of soft-matter quasicrystals and their approximants, Proc. Natl. Acad. Sci. USA 108 (2011) 20935–20940, doi:10.1073/pnas.1019763108.
- [77] G. Ungar, Y. Liu, X. Zeng, V. Percec, W.-D. Cho, Giant supramolecular liquid crystal lattice, Science 299 (2003) 1208–1211, doi:10.1126/science.1078849.
- [78] X. Zeng, G. Ungar, Y. Liu, V. Percec, A.E. Dulcey, J.K. Hobbs, Supramolecular dendritic liquid quasicrystals, Nature 428 (2004) 157–160, doi:10.1038/ nature02368.
- [79] S. Lee, M.J. Bluemle, F.S. Bates, Discovery of a Frank-Kasper σ phase in sphere-forming block copolymer melts, Science 330 (2010) 349–353, doi:10.1126/science.1195552.
- [80] M. Peterca, V. Percec, Recasting metal alloy phases with block copolymers, Science 330 (2010) 333–334, doi:10.1126/science.1196698.
- [81] T.M. Gillard, S. Lee, F.S. Bates, Dodecagonal quasicrystalline order in a diblock copolymer melt, Proc. Natl. Acad. Sci. USA 113 (2016) 5167–5172, doi:10.1073/ pnas.1601692113.
- [82] K. Kim, M.W. Schulze, A. Arora, R.M. Lewis, M.A. Hillmyer, K.D. Dorfman, F.S. Bates, Thermal processing of diblock copolymer melts mimics metallurgy, Science 356 (2017) 520–523, doi:10.1126/science.aam7212.
- [83] D.V. Perroni, M.K. Mahanthappa, Inverse Pm3n cubic micellar lyotropic phases from zwitterionic triazolium gemini surfactants, Soft Matter. 9 (2013) 7919– 7922, doi:10.1039/C3SM51238J.
- [84] S.A. Kim, K.-J. Jeong, A. Yethiraj, M.K. Mahanthappa, Low-symmetry sphere packings of simple surfactant micelles induced by ionic sphericity, Proc. Natl. Acad. Sci. USA 114 (2017) 4072–4077, doi:10.1073/pnas.1701608114.
- [85] C.M. Baez-Cotto, M.K. Mahanthappa, Micellar mimicry of intermetallic C14 and C15 laves phases by aqueous lyotropic self-assembly, ACS Nano 12 (2018) 3226– 3234, doi:10.1021/acsnano.7b07475.
- [86] M. Huang, C.-H. Hsu, J. Wang, S. Mei, X. Dong, Y. Li, M. Li, H. Liu, W. Zhang, T. Aida, W.-B. Zhang, K. Yue, S.Z.D. Cheng, Selective assemblies of giant tetrahedra via precisely controlled positional interactions, Science 348 (2015) 424–428, doi:10.1126/science.aaa2421.
- [87] X. Feng, R. Zhang, Y. Li, Y. Hong, D. Guo, K. Lang, K.-Y. Wu, M. Huang, J. Mao, C. Wesdemiotis, Y. Nishiyama, W. Zhang, W. Zhang, T. Miyoshi, T. Li, S.Z.D. Cheng, Hierarchical self-organization of AB_n dendron-like molecules into a supramolecular lattice sequence, ACS Cent. Sci. 3 (2017) 860–867, doi:10.1021/acscentsci.7b00188.
- [88] K. Yue, M. Huang, R.L. Marson, J. He, J. Huang, Z. Zhou, J. Wang, C. Liu, X. Yan, K. Wu, Z. Guo, H. Liu, W. Zhang, P. Ni, C. Wesdemiotis, W.-B. Zhang, S.C. Glotzer, S.Z.D. Cheng, Geometry induced sequence of nanoscale Frank–Kasper and quasicrystal mesophases in giant surfactants, Proc. Natl. Acad. Sci. USA 113 (2016) 14195–14200, doi:10.1073/pnas.1609422113.
- [89] Z. Su, C.-H. Hsu, Z. Gong, X. Feng, J. Huang, R. Zhang, Y. Wang, J. Mao, C. Wesdemiotis, T. Li, S. Seifert, W. Zhang, T. Aida, M. Huang, S.Z.D. Cheng, Identification of a Frank–Kasper Z phase from shape amphiphile self-assembly, Nat. Chem. 11 (2019) 899–905, doi:10.1038/s41557-019-0330-x.
- [90] M. Girard, S. Wang, J.S. Du, A. Das, Z. Huang, V.P. Dravid, B. Lee, C.A. Mirkin, M.O. de la Cruz, Particle analogs of electrons in colloidal crystals, Science 364 (2019) 1174–1178, doi:10.1126/science.aaw8237.
- [91] K.K. Lachmayr, C.M. Wentz, L.R. Sita, An exceptionally stable and scalable sugar-polyolefin Frank-Kasper A15 phase, Angew. Chem. Int. Ed. 59 (2020) 1521–1526, doi:10.1002/anie.201912648.
- [92] K.K. Lachmayr, L.R. Sita, Small-molecule modulation of soft-matter Frank-Kasper phases: a method for adding function to form, Angew. Chem. Int. Ed. 59 (2020) 3563–3567, doi:10.1002/anie.201915416.
- [93] C. Roche, V. Percec, Complex adaptable systems based on self-assembling dendrimers and dendrons: toward dynamic materials, Isr. J. Chem. 53 (2013) 30–44, doi:10.1002/ijch.201200099.

- [94] M. Peterca, V. Percec, M.R. Imam, P. Leowanawat, K. Morimitsu, P.A. Heiney, Molecular structure of helical supramolecular dendrimers, J. Am. Chem. Soc. 130 (2008) 14840–14852, doi:10.1021/ja806524m.
- [95] B.M. Rosen, M. Peterca, C. Huang, X. Zeng, G. Ungar, V. Percec, Deconstruction as a strategy for the design of libraries of self-assembling dendrons, Angew. Chem. Int. Ed. 49 (2010) 7002–7005, doi:10.1002/anie.201002514.
- [96] Y.K. Kwon, S. Chvalun, A.-I. Schneider, J. Blackwell, V. Percec, J.A. Heck, Supramolecular tubular structures of a polymethacrylate with tapered side groups in aligned hexagonal phases, Macromolecules 27 (1994) 6129–6132, doi:10.1021/ma00099a029.
- [97] Y.K. Kwon, S.N. Chvalun, J. Blackwell, V. Percec, J.A. Heck, Effect of temperature on the supramolecular tubular structure in oriented fibers of a poly(methacrylate) with tapered side groups, Macromolecules 28 (1995) 1552– 1558, doi:10.1021/ma00109a029.
- [98] V. Percec, D. Schlueter, G. Ungar, S. Z. D. Cheng, A. Zhang, Hierarchical control of internal structure, diameter and stability of supramolecular and macromolecular columns generated from tapered monodendritic building blocks, Macromolecules 31 (1998) 1745–1762, doi:10.1021/ma971459p.
- [99] C. Pugh, V. Percec, Columnar mesophases of cyclic trimers of disubstituted acetylenes, J. Mater. Chem. 1 (1991) 765–773, doi:10.1039/JM9910100765.
- [100] V. Percec, J. Heck, M. Lee, G. Ungar, A. Alvarez-Castillo, Poly{2-vinyloxyethyl 3, 4, 5-tris[4-(n-dodecanyloxy)benzyloxy]benzoate]: a self-assembled supramolecular polymer similar to tobacco mosaic virus, J. Mater. Chem. 2 (1992) 1033–1039, doi:10.1039/JM9920201033.

- [101] V. Percec, A.E. Dulcey, M. Peterca, M. Ilies, S. Nummelin, M.J. Sienkowska, P.A. Heiney, Principles of self-assembly of helical pores from dendritic dipeptides, Proc. Natl. Acad. Sci. USA 103 (2006) 2518–2523, doi:10.1073/pnas. 0509676103.
- [102] V. Percec, M. Glodde, T.K. Bera, Y. Miura, I. Shiyanovskaya, K.D. Singer, V.S.K. Balagurusamy, P.A. Heiney, I. Schnell, A. Rapp, H.-W. Spiess, S.D. Hudson, H. Duan, Self-organization of supramolecular helical dendrimers into complex electronic materials, Nature 419 (2002) 384–387, doi:10.1038/nature01072.
- [103] V. Percec, A.E. Dulcey, V.S.K. Balagurusamy, Y. Miura, J. Smidrkal, M. Peterca, S. Nummelin, U. Edlund, S.D. Hudson, P.A. Heiney, H. Duan, S.N. Magonov, S.A. Vinogradov, Self-assembly of amphiphilic dendritic dipeptides into helical pores, Nature 430 (2004) 764–768, doi:10.1038/nature02770.
- [104] C. Roche, H.-J. Sun, P. Leowanawat, F. Araoka, B.E. Partridge, M. Peterca, D.A. Wilson, M.E. Prendergast, P.A. Heiney, R. Graf, H.W. Spiess, X. Zeng, G. Ungar, V. Percec, A supramolecular helix that disregards chirality, Nat. Chem. 8 (2016) 80–89, doi:10.1038/nchem.2397.
- [105] B.E. Partridge, L. Wang, D. Sahoo, J.T. Olsen, P. Leowanawat, C. Roche, H. Ferreira, K.J. Reilly, X. Zeng, G. Ungar, P.A. Heiney, R. Graf, H.W. Spiess, V. Percec, Sequence-defined dendrons dictate supramolecular cogwheel assembly of dendronized perylene bisimides, J. Am. Chem. Soc. 141 (2019) 15761–15766, doi:10.1021/jacs.9b08714.